Cell Reports

Article

Histone chaperone FACT complex coordinates with HIF to mediate an expeditious transcription program to adapt to poorly oxygenated cancers

Graphical abstract

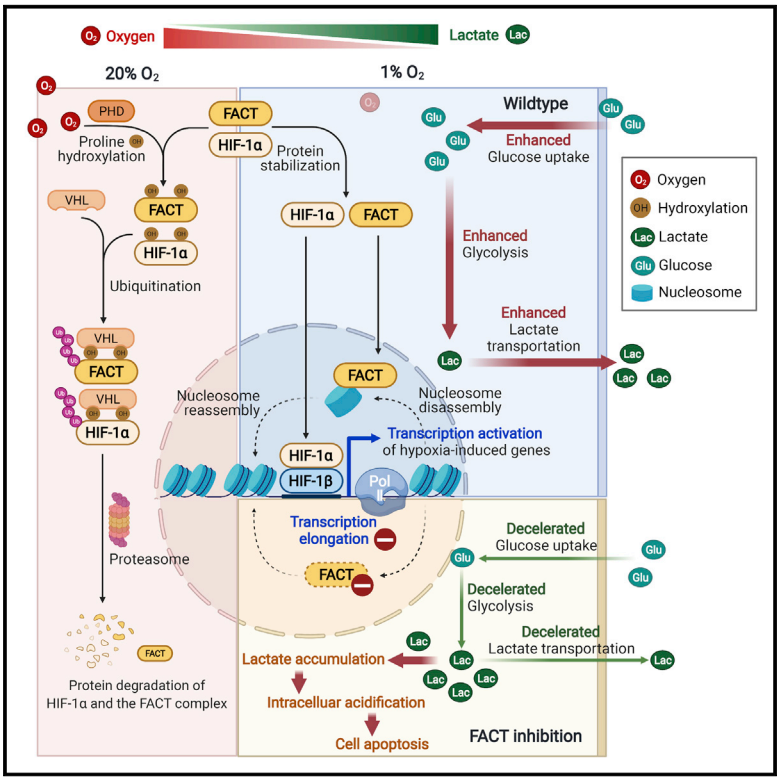

Highlights

- Cancer cells rely on the FACT complex to survive under hypoxic stress
- PHD/VHL axis regulates the protein stability of the FACT complex
- The FACT complex enables HIF-mediated metabolic reprogramming in cancer cells
- Targeting the FACT complex is an effective therapeutic approach for hypoxic tumors

Authors

Jialing Shen, Chunxue Yang, Misty Shuo Zhang, ..., Irene Oi-Lin Ng, Carmen Chak-Lui Wong, Chun-Ming Wong

Correspondence

carmencl@pathology.hku.hk (C.C.-L.W.), jackwong@pathology.hku.hk (C.-M.W.)

In brief

Shen et al. identify the histone chaperone FACT complex as an important regulator for hypoxia adaptation in cancer cells. The FACT complex facilitates HIF-initiated transcription, and inhibition of the FACT complex leads to intracellular acidification and cellular apoptosis. The FACT complex is a targetable vulnerability to combat hypoxic tumors.

Shen et al., 2022, Cell Reports *38*, 110304
February 1, 2022
https://doi.org/10.1016/j.celrep.2022.110304

CellPress

Cell Reports

CellPress
OPEN ACCESS

Article

Histone chaperone FACT complex coordinates with HIF to mediate an expeditious transcription program to adapt to poorly oxygenated cancers

Jialing Shen,[1] Chunxue Yang,[1] Misty Shuo Zhang,[1] Don Wai-Ching Chin,[1] For-Fan Chan,[1] Cheuk-Ting Law,[1] Gengchao Wang,[1] Carol Lai-Hung Cheng,[1] Mengnuo Chen,[1] Rebecca Ting-Chi Wan,[1] Mengjie Wu,[1] Zhijian Kuang,[1] Rakesh Sharma,[2] Terence Kin Wah Lee,[3] Irene Oi-Lin Ng,[1] Carmen Chak-Lui Wong,[1,*] and Chun-Ming Wong[1,4,*]

[1]State Key Laboratory of Liver Research and Department of Pathology, Li Ka Shing Faculty of Medicine, The University of Hong Kong, Pok Fu Lam, Hong Kong

[2]Proteomic and Metabolic Core Facility, Li Ka Shing Faculty of Medicine, The University of Hong Kong, Pok Fu Lam, Hong Kong

[3]Department of Applied Biology and Chemical Technology, Hong Kong Polytechnic University, Hung Hom, Hong Kong

[4]Lead contact

*Correspondence: carmencl@pathology.hku.hk (C.C.-L.W.), jackwong@pathology.hku.hk (C.-M.W.)

https://doi.org/10.1016/j.celrep.2022.110304

SUMMARY

Cancer cells adapt to hypoxia through HIFs (hypoxia-inducible factors), which initiate the transcription of numerous genes for cancer cell survival in the hypoxia microenvironment. In this study, we find that the FACT (facilitates chromatin transcription) complex works cooperatively with HIFs to facilitate the expeditious expression of HIF targets for hypoxia adaptation. Knockout (KO) of the FACT complex abolishes HIF-mediated transcription by impeding transcription elongation in hypoxic cancer cells. Interestingly, the FACT complex is post-translationally regulated by PHD/VHL-mediated hydroxylation and proteasomal degradation, in similar fashion to HIF-1/2α. Metabolic tracing confirms that FACT KO suppresses glycolytic flux and impairs lactate extrusion, leading to intracellular acidification and apoptosis in cancer cells. Therapeutically, hepatic artery ligation and anti-angiogenic inhibitors adversely induce intratumoral hypoxia, while co-treatment with FACT inhibitor curaxin remarkably hinders the growth of hypoxic tumors. In summary, our findings suggest that the FACT complex is a critical component of hypoxia adaptation and a therapeutic target for hypoxic tumors.

INTRODUCTION

Nucleosomes, 146-bp DNA-wrapped core histone octamers, are the fundamental unit of eukaryotic chromatin. The local density and distribution of nucleosomes within a chromosomal region determine the chromatin structure. Nucleosome density and distribution could be affected by many factors, which mainly include DNA methylation status, histone modification signatures, and chromatin remodeling complex activities. In fact, nucleosomes are dynamically assembled and disassembled throughout the cell cycle. The dynamic nucleosome-recycling processes are regulated by various histone chaperones, which mediate the histone transportation, disposition, and removal as well as replacement of histone variants. These histone chaperone proteins are known to be crucial for different nucleosome-reorganization events during DNA replication, DNA damage repair, and gene transcription.

The facilitates chromatin transcription (FACT) complex is a heterodimeric histone chaperone complex that comprises two core subunits, structure-specific recognition protein 1 (SSRP1) and suppressor of Ty 16 (SUPT16H) (Orphanides et al., 1999). The FACT complex plays a critical role in transcription initiation, transcription elongation, DNA replication, and DNA repair (Carrozza et al., 2003). Mechanistically, the FACT complex functions to mediate the disassembly and reassembly of nucleosomes, thereby allowing the passage of RNA polymerase II through the chromatin during gene transcription (Belotserkovskaya et al., 2003). The FACT complex is lowly expressed in differentiated somatic cells but abundantly expressed in undifferentiated cells and stem cells (Garcia et al., 2011, 2013). The FACT complex is found to regulate the stemness properties of undifferentiated cells by modulating stemness gene expression signatures (Garcia et al., 2011, 2013). Recently, upregulation of the FACT complex is observed in multiple human cancers. Overexpression of the FACT complex was associated with aggressive clinical features and poor prognosis (Garcia et al., 2013). Particularly, the FACT complex is essential for the activation of nuclear factor κB (NF-κB) signaling in non-small cell lung carcinoma (NSCLC) and participated in the feedforward loop of Myc signaling in neuroblastoma (Carter et al., 2015a; Gasparian et al., 2011). Previously, we showed that the FACT complex was frequently upregulated in human hepatocellular carcinoma (HCC) and was associated with cancer aggressiveness. Inactivation of the FACT complex remarkably suppressed HCC cell proliferation

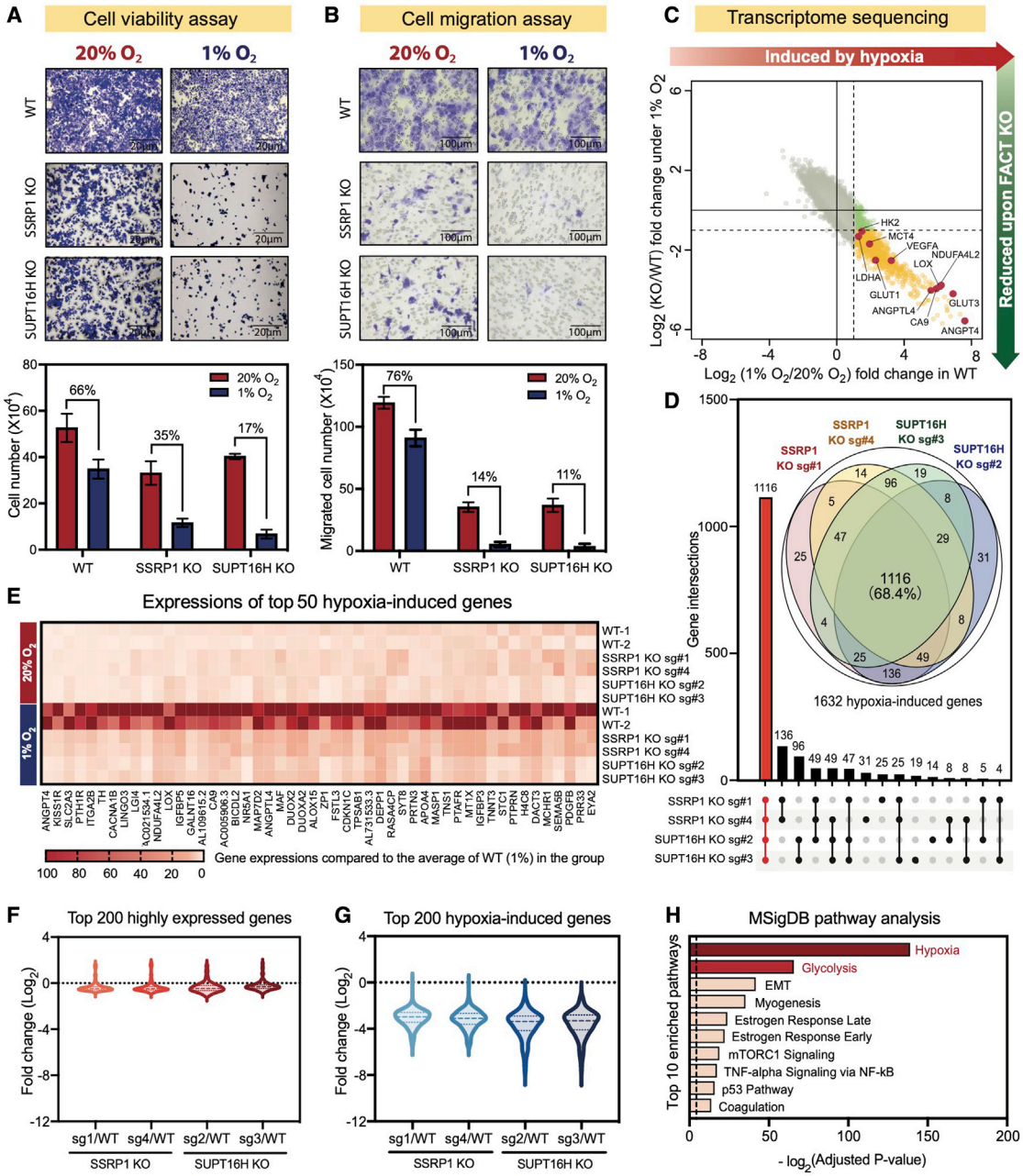

Figure 1. The histone chaperone FACT complex mediates cancer cell adaptation to hypoxic stress

(A and B) Wild-type (WT), SSRP1 knockout (KO), and SUPT16H KO MHCC97L cells were cultured in normoxia (20% O_2) and hypoxia (1% O_2) conditions for 48 h.

(A) Cell viability was determined by crystal violet staining and cell counting. (B) Cell migration was determined by transwell migration assay.

(C) Transcriptome changes of two replicates of MHCC97L WT, SSRP1 KO (sg1 and sg4), and SUPT16H KO (sg2 and sg3) cultured in normoxia and hypoxia for 24 h were detected by RNA-seq. x axis represents the mean fold change between hypoxia and normoxia in two replicas of WT cells. y axis represents the average fold change between WT and the FACT complex KO cells (mean of SSRP1 KO sg1 and sg4 and SUPT16H KO sg2 and sg3) in hypoxia.

(D) Venn diagram showing the overlapping of downregulated hypoxia-induced genes (fold change >2) in each stable KO clone. Upset plot depicts the number of unique and shared genes identified in each samples.

(E) Expressions of the key hypoxia-induced genes in WT and the FACT complex KO cells in normoxia and hypoxia were detected by RNA-seq. Gene expression was normalized to the mean of two WT replicas in 1% O_2 as 100%.

(F) A reduction of gene expressions was observed in the top 200 most abundantly expressed genes when SSRP1 or SUPT16H was knocked out.

(G) Expressions of top 200 hypoxia-induced genes were drastically decreased upon the FACT complex KO under hypoxic stress.

(legend continued on next page)

and migration *in vitro* as well as HCC tumorigenicity and lung metastasis *in vivo* (Shen et al., 2020). Targeting the FACT complex by a novel small molecular inhibitor curaxin demonstrated a promising anticancer effect in NSCLC, pancreatic cancer, breast cancer, neuroblastoma, and HCC (Carter et al., 2015a; Gasparian et al., 2011; Shen et al., 2020). However, the mechanistic implications of the FACT complex in human cancer have not been fully investigated. Interestingly, we recently reported that the FACT complex facilitates the transcription of NRF2-target genes and is essential for HCC cells to survive under oxidative stress. Based on this observation, we hypothesized that the FACT complex may play an imperative role in various adaptive responses of cancer cells.

Hypoxia (O_2 deprivation) is a common feature of human cancers. Hypoxia stabilizes hypoxia-inducible factor 1 (HIF-1), a transcription factor that promptly activates the transcription of two classes of genes: (1) genes that allow cancer cells to survive hypoxia (metabolic reprogramming) and (2) genes that further confer cancer cells' aggressive properties (self-renewability, metastasis, angiogenesis, and therapeutic resistance). Most studies in the past decades focused on the mechanisms of HIF-1 stabilization, identification of HIF-1 target genes, and the revelation of new oncogenic functions of HIF-1. Transcriptional programming of HIF-1 has to be swifted due to the instant depletion of O_2, which is the most essential nutrient for cell survival. Therefore, the molecular mechanisms that enable HIF-1 to activate transcription expeditiously are of crucial importance but have not been clearly addressed. Herein, we demonstrated that the nucleosome reorganization controlled by the histone chaperone FACT complex plays an important role in supporting the fast transcription program instigated by HIFs. Our study highlighted the vital role of the FACT complex in cancer hypoxia adaption, which could be exploited for novel cancer therapeutic regime, especially in combination with anti-angiogenic strategies.

RESULTS

Histone chaperone FACT complex controls the transcriptional program of hypoxic cancer cells

HIFs are the transcription factors that initiate the transcription of a cascade of genes in hypoxia. This transcriptional program is expeditious, enabling cells to adapt quickly to hypoxia. However, transcription initiation only represents the first step of gene expression. We sought to understand how the FACT complex mediates transcription elongation to support the rapid transcriptional program in cancer cells under hypoxia. To explore the roles of the FACT complex during hypoxic adaptation in cancer, we stably knocked out the two subunits of the FACT complex, SSRP1 and SUPT16H, in HCC cell line MHCC97L with two single-guide RNAs (sgRNAs), respectively. Knockout (KO) efficiencies are validated through western blots (Figure S1A). Tracking of indels by decomposition (TIDE) analysis of Sanger sequencing further confirmed the CRISPR-induced indels in the FACT KO clones (Figure S1B). In addition, we also established SSRP1 and SUPT16H KO clones in a broad spectrum of human cancer cell lines, including liver cancer (Huh-7), colorectal cancer (HCT116), breast cancer (MDA-MB-231), cervical cancer (HeLa), and ovarian cancer (ES2) cells (Figure S1C). Consistent with our previous report, we found that the protein stabilities of the two heterodimeric subunits, SSRP1 and SUPT16H, are mutually dependent. KO of either SSRP1 or SUPT16H resulted in a complete depletion of the FACT complex (Figures S1A and S1C). Phenotypically, inactivation of the FACT complex by either SSRP1 KO (subclone sg#1) or SUPT16H KO (subclone sg#2) or treatment with a small molecular FACT complex inhibitor (curaxin) profoundly suppressed the viability and mobility of cancer cells in hypoxia condition (1% O_2) as compared with normoxia condition (20% O_2; Figures 1A and 1B; Figures S2A–S2C). These findings indicated that the FACT complex is indispensable for cancer cells to survive in hypoxic stress. To further elucidate the molecular mechanism by which the FACT complex confers hypoxic cancer cells' growth advantages, we studied the transcriptomes of wild-type (WT), SSRP1 KO (subclone sg#1 and sg#4), and SUPT16H KO (subclone sg#2 and sg#3) MHCC97L cells that were exposed to 20% O_2 and 1% O_2 by transcriptome sequencing (RNA sequencing [RNA-seq]). We noticed that the mRNA expression of a great number of hypoxia-induced genes (68.4%; 1,116 out of 1,632) were repressed in both SSRP1 and SUPT16H KO subclones as compared with WT MHCC97L in hypoxia (Figures 1C and 1D). These genes include, but are not limited to, well-known HIF transcriptional targets VEGFA, ANGPTL4, LOX, NDUFA4L2, and CA9 that play important roles in angiogenesis, lipid metabolism, extracellular matrix modification, mitochondrial activity, glucose metabolism, and metastasis (Figures 1C and IE). qRT-PCR confirmed the RNA-seq data and further showed that the FACT complex inhibitor, curaxin, recapitulated the results of SSRP1 or SUPT16H KO (Figures S3A–S3C). Different from the hypoxia-induced genes, mRNA expressions of HIF1A, HIF2A, and HIF1B remained predominantly unchanged in hypoxia and were not regulated by the FACT complex (Figures S3D and S3E). Considering the role of the FACT complex in transcription elongation, we analyzed the top 200 most abundantly expressed genes (Figure 1F) and the top 200 hypoxia-induced genes (Figure 1G) in WT, SSRP1 KO, and SUPT16H KO subclones. Gene expressions of the highly expressed genes were slightly suppressed upon SSRP1 or SUPT16H KO as expected (Figure 1F). In comparison, the reduction magnitude of hypoxia-induced genes was more drastic, suggesting a specific role of the FACT complex in modulating the expression of hypoxia-inducible genes during hypoxic adaptation (Figure 1G). To further explore whether the FACT complex's regulation is specific to HIF1A- or HIF2A-mediated transcription activation, we knockdown HIF-1A or HIF-2A in the FACT complex KO subclones (Figure S3F). The result shows that KO of the FACT complex abolished the transcription of hypoxia-inducible genes

(H) MSigDB canonical pathway enrichment analysis was performed in 1,116 overlapped genes that were upregulated by hypoxia and downregulated commonly in the four FACT complex KO clones.

Results suggested hypoxia and glycolysis as the top-ranked pathways that were regulated by the FACT complex under hypoxic stress. (A and B) Data represent the mean ± SD from triplicate experiments. See also Figures S1–S3.

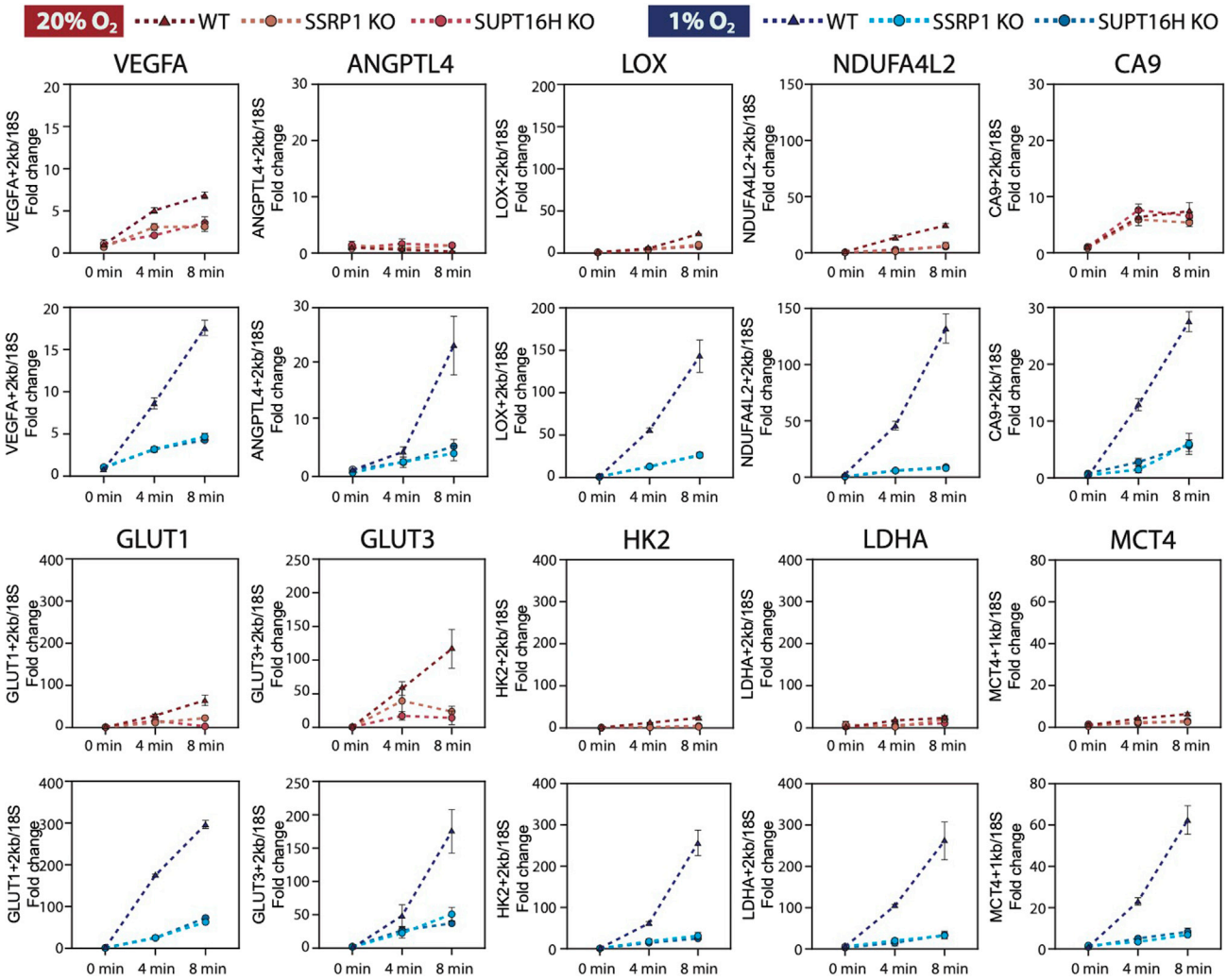

Figure 2. The FACT complex facilitates transcription elongation of hypoxia-induced genes

Transcription elongation rate was determined by 4sU-DRB assay. The transcription elongation rates of hypoxia marker genes VEGFA, ANGPTL4, LOX, NDUFA4L2, and CA9 and hypoxia-induced metabolic genes GLUT1, GLUT3, HK2, LDHA, and MCT4 were remarkably increased in hypoxia and were drastically abolished in the FACT complex KO cells. Data represent the mean ± SD from triplicate experiments.

initiated by both HIF1A and HIF2A as well as those initiated by HIF1A alone, suggesting a central role of the FACT complex in HIF-induced gene expression (Figures S3G and S3H).

The FACT complex is responsible for transcription elongation of hypoxic cancer cells

Considering the role of the FACT complex as a histone chaperone, we speculated that it directly regulates the transcription elongation of the HIF transcriptional targets by enabling the rapid passage of RNA polymerase II (Pol II) through the chromatin. To this end, we performed 4sU-DRB assay to measure RNA elongation rate. DRB was first added to cells to capture RNA Pol II at the transcription start site to halt RNA elongation. After removal of DRB, 4sU was added to label all nascent RNA followed by biotin-streptavidin immunoprecipitation of nascent RNA (Fuchs et al., 2015). Within 0, 4, and 8 min upon addition of 4sU, we collected the newly synthesized RNA from MHCC97L-WT, SSRP1 KO, and SUPT16H KO subclones exposed to 20% and 1% O_2 for qRT-PCR to determine the transcription elongation rates of gene of interests. We found that the transcription elongation rates of the classical HIF-transcriptional targets, including VEGFA, ANGPTL4, LOX, NDUFA4L2, and CA9, were remarkably increased by hypoxia (Figure 2). However, decelerated transcription elongation rates could be observed in the FACT complex KO cells and was especially apparent in 1% O_2 (Figure 2). Consistently, hypoxia accelerated the transcription elongation of the key HIF-induced and glycolysis-related genes, including GLUT1, GLUT3, HK2, lactate dehydrogenase A (LDHA), and MCT4, and this acceleration was markedly perturbed by the KO of the FACT complex in HCC cells (Figure 2). Taken together, these findings further sustained our hypothesis that HIF-1 controls the initiation, while the FACT complex supports the elongation of rapid transcriptional program in cancer cells during hypoxic adaptation.

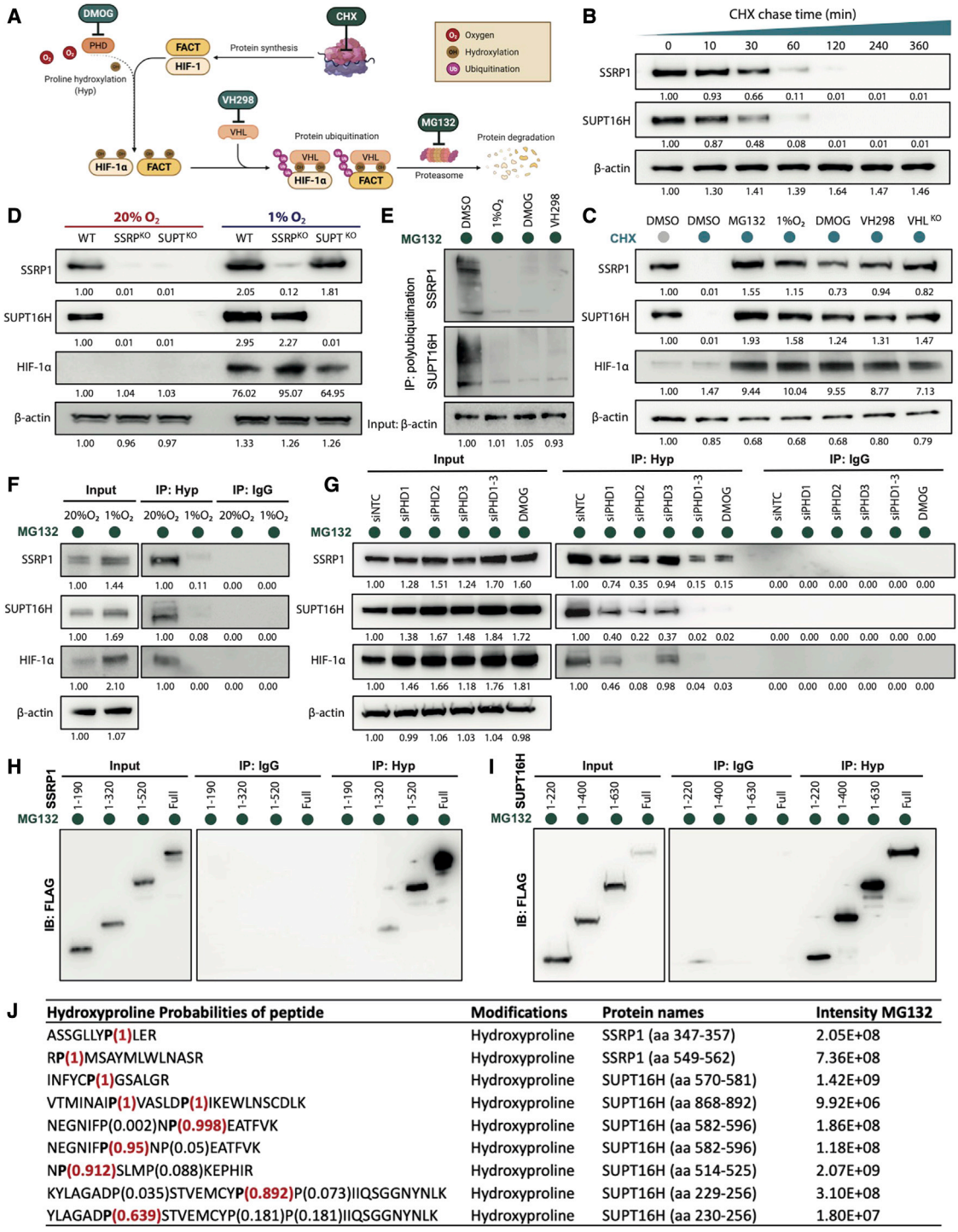

J

Hydroxyproline Probabilities of peptide	Modifications	Protein names	Intensity MG132
ASSGLLYP(1)LER	Hydroxyproline	SSRP1 (aa 347-357)	2.05E+08
RP(1)MSAYMLWLNASR	Hydroxyproline	SSRP1 (aa 549-562)	7.36E+08
INFYCP(1)GSALGR	Hydroxyproline	SUPT16H (aa 570-581)	1.42E+09
VTMINAIP(1)VASLDP(1)IKEWLNSCDLK	Hydroxyproline	SUPT16H (aa 868-892)	9.92E+06
NEGNIFP(0.002)NP(0.998)EATFVK	Hydroxyproline	SUPT16H (aa 582-596)	1.86E+08
NEGNIFP(0.95)NP(0.05)EATFVK	Hydroxyproline	SUPT16H (aa 582-596)	1.18E+08
NP(0.912)SLMP(0.088)KEPHIR	Hydroxyproline	SUPT16H (aa 514-525)	2.07E+09
KYLAGADP(0.035)STVEMCYP(0.892)P(0.073)IIQSGGNYNLK	Hydroxyproline	SUPT16H (aa 229-256)	3.10E+08
YLAGADP(0.639)STVEMCYP(0.181)P(0.181)IIQSGGNYNLK	Hydroxyproline	SUPT16H (aa 230-256)	1.80E+07

Figure 3. The FACT complex is hydroxylated and degraded through PHD/VHL axis

(A) An illustration demonstrating the post-translational regulation of the FACT complex and HIF-1α under normoxia. CHX (protein synthesis inhibitor), DMOG (PHD inhibitor), VH298 (VHL inhibitor), and MG132 (proteasome inhibitor) were used in the experiments.

(B) MHCC97L was treated with 100 μg/mL CHX, and proteins were collected at 0, 10, 30, 60, 120, 240, and 360 min for western blot analysis. SSRP1 and SUPT16H degraded within 120 min after CHX treatment.

(C) MHCC97L was exposed to MG132, 1% O_2, DMOG, or VH298 or transfected with CRISPR RNA (crRNA) targeting VHL to knock out VHL. The above treatments stabilized SSRP1 and SUPT16H proteins in the presence of 100 μg/mL CHX at 6 h.

(legend continued on next page)

Hydroxylation, ubiquitination, and protein degradation of the FACT complex through PHD/VHL axis

Besides transcriptional control, cancer cells have developed coordinated mechanisms at post-translational level to cope with hypoxic stress. Under normoxia conditions, HIF-1/2α is hydroxylated by prolyl-hydroxylases (PHDs) (Epstein et al., 2001), facilitating the binding of von Hippel-Lindau (VHL), which polyubiquitinates HIF-1/2α for protein degradation through proteasome (Kaelin and Ratcliffe, 2008). In hypoxia, the PHD/VHL axis is inactivated, leading to the stabilization of HIF-1/2α. Previously, a large-scale mapping of VHL-interacted proteins showed the protein-protein interaction between SUPT16H and VHL (Lopez et al., 2015). Considering the vital role of the FACT complex during hypoxia response, we speculated the protein stability of the FACT complex is also regulated by the PHD/VHL axis and hypoxic stress (Figure 3A). To validate our hypothesis, we first inhibited total protein synthesis by cycloheximide (CHX) in MHCC97L cells and found that both SSRP1 and SUPT16H exhibited a fast degradation rate as compared with the housekeeping gene β-actin (Figure 3B). Interestingly, a proteasomal inhibitor (MG132), hypoxic stress (1% O_2), a PHD competitive inhibitor (DMOG), a VHL inhibitor (VH298), and direct KO of VHL all restored SSRP1 and SUPT16H protein expressions, even in the presence of CHX (Figures 3A–3C), suggesting that protein stability of the FACT complex, like HIF-1/2α, is likely to be regulated by PHD-mediated hydroxylation, VHL-mediated ubiquitination, and proteasome-mediated degradation (Semenza, 2001). We previously showed that KO of either subunit of the FACT complex led to protein degradation of the untargeted subunit and the untargeted subunit could be stabilized upon the inhibition of proteasome activities (Shen et al., 2020). Strikingly, we found that hypoxic stress could also stabilize SSRP1 and SUPT16H, even when the other subunit is depleted in MHCC97L cells (Figure 3D). Similarly, silencing of VHL by either VH298 or CRISPR Alt-R system could also reiterate the effects of hypoxia in stabilizing SSRP1 and SUPT16H (Figures S4A and S4B), suggesting VHL also plays a role in the proteasome-mediated degradation of SSRP1 and SUPT16H. Considering the vital role of VHL in HIF-1/2α ubiquitination, we further examined whether VHL could also mediate the ubiquitination of the FACT complex. We showed that depletion of either SSRP1 or SUPT16H will increase ubiquitination of the other subunit (Figure S4C), while hypoxia and silencing of VHL inhibited the polyubiquitination of SSRP1 and SUPT16H (Figure 3E; Figure S4D). Furthermore, inhibition of PHD activities by DMOG showed similar phenotypes on regulating SSRP1/SUPT16H protein ubiquitination and stabilization (Figure 3E). This evidence prompted us to further ask whether SSRP1 and SUPT16H, like HIF-1/2α, are hydroxylated at the proline residues by PHDs. To this end, we performed immunoprecipitation (IP) with anti-hydroxyproline (Hyp) antibody, which was able to pull down both subunits of the FACT complex under 20% O_2. As expected, only low level of hydroxylated SSRP1 and SUPT16H proteins could be detected in 1% O_2, given O_2 provides the co-substrates for hydroxylation (Figure 3F). Silencing of PHD1–3 by small interfering RNA (siRNA) or DMOG further demonstrated that PHDs were involved in the proline hydroxylation of SSRP1 and SUPT16H (Figure 3G). To investigate which proline residues were hydroxylated among SSRP1 and SUPT16H, we constructed and transiently expressed a series of FLAG-tagged SSRP1 and SUPT16H truncated proteins in HEK293 cells. Through IP of hydroxyproline proteins and immunoblotting of FLAG-tagged SSRP1 and SUPT16H truncated proteins, we confirmed that the hydroxylated prolines are enriched at one end of SSRP1 (Figure 3H), whereas hydroxylated proline residues can be detected at full-length fragments of SUPT16H (Figure 3I). To further confirm the detailed hydroxyproline sites on the FACT complex, FLAG-tagged SSRP1 and SUPT16H proteins were transiently expressed in HEK293 cells, followed by MG132 treatment together with or without DMOG. Proteins were then purified through FLAG-IP and gel purifications. Liquid chromatography-tandem mass spectrometry (LC-MS/MS) revealed two possible hydroxylated proline residues on SSRP1 (Pro^{354} and Pro^{550}) and eight possible proline residues on SUPT16H (Pro^{236}, Pro^{244}, Pro^{515}, Pro^{575}, Pro^{588}, Pro^{590}, Pro^{875}, and Pro^{881}), consistently with the truncation models (Figure 3J). Size shift on the proline residues of both proteins was also confirmed by MS, and a representative MS spectrum is shown for demonstration (Figures S4F and S4G). Taken together, we concluded that the FACT complex is likely to be prolyl-hydroxylated by PHDs in the presence of O_2, enabling the recognition of VHL for poly-ubiquitination, which leads to proteasomal degradation, like HIF-1/2α (Figure 3A).

The FACT complex facilitates metabolically reprograming in cancer cells and prevents intracellular acidification

Under poorly oxygenated conditions, HIF-1 allows cells to adapt by transcriptionally activating genes to accelerate glycolysis and

(D) SSRP1 protein expression was lost upon SUPT16H KO and vice versa. Protein degradation of either subunit of the FACT complex could be largely blocked upon 1% O_2 exposure.
(E) Polyubiquitin pull-down assay confirmed the ubiquitination of both SSRP1 and SUPT16H in MHCC97L cells upon the treatment of 8 μM MG132 for 8 h. The ubiquitination of both SSRP1 and SUPT16H ubiquitination was significantly inhibited upon hypoxia, DMOG, and VH298 treatments.
(F) Immunoprecipitation was performed with anti-hydroxyproline (Hyp) antibody in MHCC97L cells exposed to normoxia and hypoxia in the presence of 8 μM MG132 for 8 h. IP of prolyl-hydroxylated proteins confirmed the proline hydroxylation on both SSRP1 and SUPT16H in normoxia. Their proline hydroxylation was inhibited under hypoxia.
(G) MHCC97L cells were transfected with siRNA targeting PHD1–3 for knockdown. After 48 h of transfection, cells were treated with 8 μM MG132 with or without DMOG for 6 h. Cells were then harvested for hydroxyproline IP and probed with SSRP1, SUPT16H, and HIF-1α antibodies. IgG, immunoglobulin G.
(H and I) The lysates of HEK293 transfected with indicated FLAG-tagged SSRP1 (H) and SUPT16H (I) constructs were subjected to immunoprecipitation with anti-Hyp antibody. The immunoprecipitated proteins were then probed with anti-FLAG antibody.
(J) HEK293 cells were overexpressed with FLAG-SSRP1 and FLAG-SUPT16H. Cells were then treated with 8 μM MG132 for 6 h and collected for FLAG IP. LC-MS/MS analysis was performed on purified SSRP1 and SUPT16H proteins.
Probabilities, modification types, peptide position, and intensity are shown as listed. (B–G) Quantification of protein levels was performed by Image Lab software v.6.1. See also Figure S4 and Table S4.

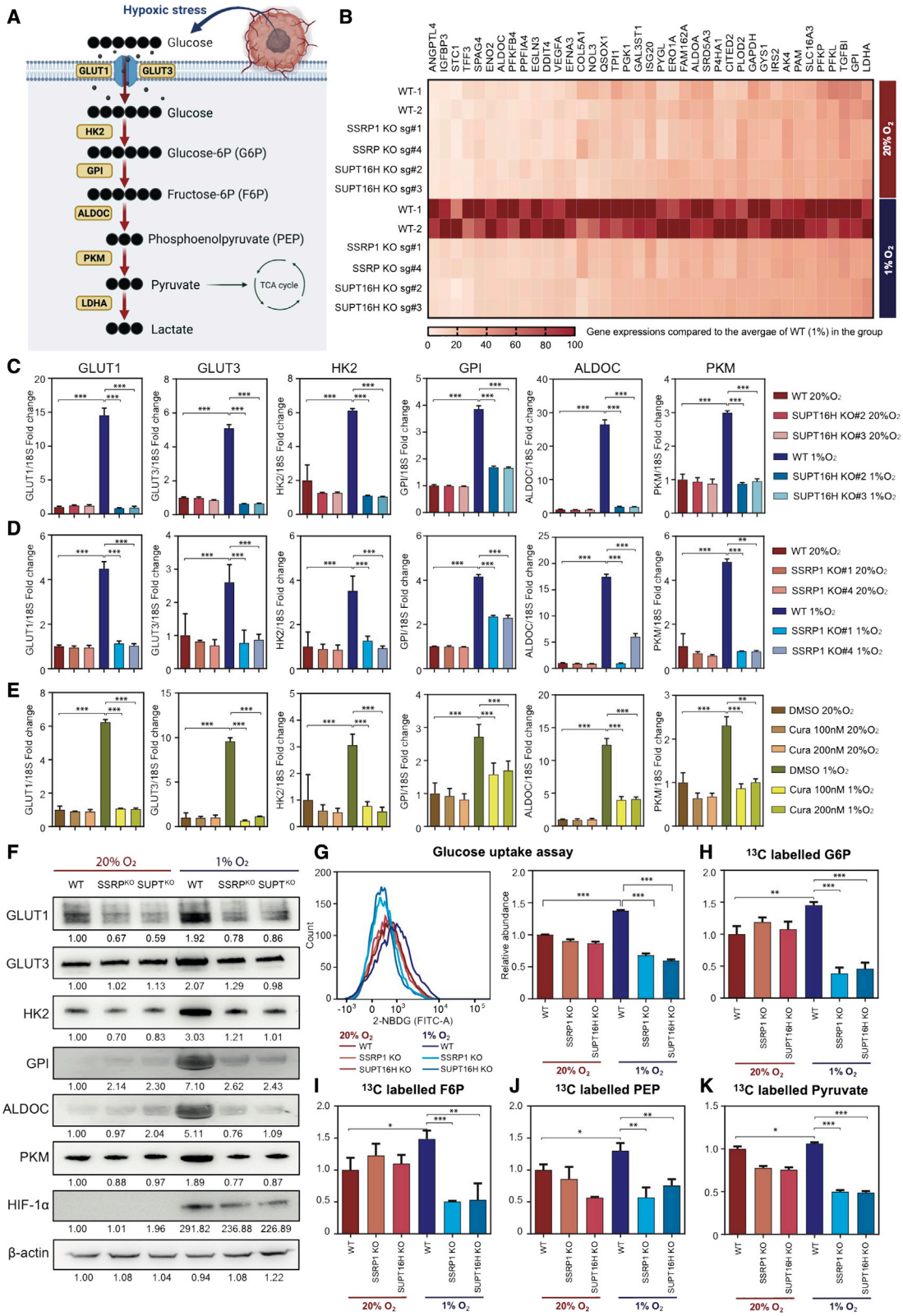

(legend on next page)

decelerate the conversion of pyruvate into acetyl-coenzyme A (CoA), which enters tricarboxylic acid (TCA) cycle and electron transport chain (Semenza, 2012). For instance, HIF-1 activates the transcription of glucose transporters (GLUT1 and GLUT3) to increase the uptake of glucose (Chen et al., 2001; Royer et al., 2000). HIF-1 also stimulates the activation of glycolytic enzymes, such as glucose-6-phosphate isomerase (GPI), Aldolase C (ALDOC), and pyruvate kinase (PKM), to accelerate glucose metabolism (Figure 4A; Wang et al., 2005; Yoon et al., 2001). LDHA then converts pyruvate into lactate to prevent pyruvate to be diverted into the TCA cycle, as well as speeding up glycolysis by regenerating NAD^+ (Figure 5A; Fantin et al., 2006; Semenza et al., 1996). In addition, HIF-1 activates the lactate transporter, monocarboxylate transporter 4 (MCT4), to pump lactate to extracellular space to prevent intracellular acidification (Sonveaux et al., 2008; Ullah et al., 2006). Our pathway analysis demonstrated that glycolysis is the top pathway being affected by the FACT complex in hypoxia (Figure 1H). The upregulation of all hypoxia-induced glycolytic enzymes in glycolysis pathway was repressed upon KO of SSRP1 and SUPT16H according to the RNA-seq data (Figure 4B). qRT-PCR and western blot further validated that hypoxia-induced expressions of glucose transporters GLUT1 and GLUT3 and glycolytic enzymes HK2, GPI, ALDOC, and PKM were diminished upon KO of SSRP1 and SUPT16H, as well as treatment with curaxin (Figures 4C–4F). Next, to confirm the metabolic functions of the FACT complex in regulating glucose uptake under hypoxic conditions, we labeled MHCC97L-WT, -SSRP1 KO, and -SUPT16H KO subclones cultured in 20% and 1% O_2 with fluorescence-labeled 2-NBDG, a glucose analog that could not be further converted by HK2 and therefore is trapped intracellularly, which indicates the amount of glucose being taken up. Silencing of either the FACT complex or HIF-1α showed a similar effect on abolishing hypoxia-induced glucose uptake rate (Figure 4G; Figure S5A). To further investigate the metabolic fate of glucose, we cultured these subclones in 20% and 1% O_2 with universally labeled ^{13}C [U-^{13}C] glucose. Hypoxia increased all ^{13}C-labeled glycolytic intermediates, including G6P, F6P, PEP, and pyruvate. Hypoxia-induced ^{13}C incorporation of glycolytic intermediates was abolished when SSRP1 or SUPT16H was knocked out (Figures 4H–4K). As anticipated, hypoxia-induced LDHA and MCT4 expression was abolished at both mRNA and protein level when SSRP1 or SUPT16H was knocked out or inactivated by curaxin (Figures 5A and 5B; Figures S5B–S5E). Strikingly, we found that hypoxia-induced accumulation of extracellular lactate was prevented in HIF-1A knockdown (KD) and SSRP1/SUPT16H KO subclones (Figure 5C; Figure S5F). More intriguingly, we noticed that production of ^{13}C-labeled lactate reduced (Figure 5D), while unlabeled and total lactate accumulated intracellularly in SSRP1 or SUPT16H KO cancer cells in hypoxic condition (Figures 5E and 5F). This is concordant with the reduction of MCT4 expression in these subclones, leading to a reduction of lactate extrusion (Figure 5C) and hence the accumulation of intracellular lactate (Figure 5F; Ullah et al., 2006). We therefore evaluated the levels of intracellular acidification with a fluorescent intracellular pH indicator. Flow cytometric and immunofluorescent analyses both indicated that the intracellular acidification levels in these subclones completely echoed with the level of intracellular lactate (Figures 5G and 5H). Accumulation of lactate inside cancer cells leads to intracellular acidification that finally causes cell apoptosis (Park et al., 1999; Todenhöfer et al., 2018). Consistently, we found that hypoxia profoundly induced extensive apoptosis when SSRP1 or SUPT16H was knocked out (Figure 5I). The above observations can be reproduced in HCC cells upon curaxin treatment (Figures S5G and S5H). Taken together, these findings demonstrated that blockage of the FACT complex abrogates glycolysis and lactate production and extrusion, resulting in hypoxic cancer cells to intracellular acidification and apoptosis.

Targeting the FACT complex as therapy for advanced cancers

Hypoxia is a typical feature in malignant tumors. In the Cancer Genome Atlas (TCGA) cohort, we noticed that the expressions of both SSRP1 and SUPT16H were well correlated with hypoxia signatures (MCT4, LDHA, HK2, GLUT1, LOX, and VEGFA) in various solid cancers, especially in liver cancer that we focused on (Figure 6A). We further validated the expression of the FACT complex in our in-house clinical samples. Upregulation of the FACT complex was detected in around half of 100 HCC patients' samples tested (Figure 6B). The expressions of SSRP1 and SUPT16H were well correlated in both tumor and non-tumor samples (Figure 6C). Moreover, besides liver cancer, the FACT complex was essential for cancer cell proliferation and colony formation in the colorectal, breast, cervical, and ovarian cancer lines we tested (Figures S6A–S6L). Interestingly, co-silencing of HIF1A and the FACT complex completely suppressed cancer cell growth in hypoxia (Figures S6M and S6N), suggesting the

Figure 4. The FACT complex promotes glucose uptake and glycolysis under hypoxic stress

(A) Hypoxia induces glycolysis by increasing the expressions of glycolytic genes and the levels of glycolytic metabolites.

(B) Expressions of glycolysis-related genes in MHCC97L-WT and the FACT complex KO cells under normoxic and hypoxic conditions detected by RNA-seq. Gene expression was normalized to the highest expression level (mean of two replicas of WT in 1% O_2) as 100%.

(C–E) qRT-PCR validated the changes of glucose transporters and glycolytic genes GLUT1, GLUT3, HK2, GPI, ALDOC, and PKM in SUPT16H KO (C), SSRP1 KO (D), and curaxin-treated (E) MHCC97L cells under normoxia and hypoxia.

(F) Western blot confirmed the induction of GLUT1, GLUT3, HK2, GPI, ALDOC, and PKM under hypoxia for 48 h, and their expressions were reduced when SSRP1 or SUPT16H was knocked out.

(G) Glucose uptake rates in WT, SSRP1 KO, and SUPT16H KO cells were determined by 2-NBDG assay under normoxia and hypoxia conditions. Hypoxia induced glucose uptake while FACT KO abolished the induction.

(H–K) Stable isotope tracing with ^{13}C-glucose showed the increased production of glycolytic metabolites G6P, F6P, PEP, and pyruvate was blocked upon KO of the FACT complex under hypoxia after 24 h.

(C–E and G–K) Data represent the mean ± SD from triplicate experiments. *$p < 0.05$; **$p < 0.01$; ***$p < 0.001$; Student's t test. (F) Quantification of protein expressions was performed by Image Lab software v.6.1. See also Figure S5 and Table S5.

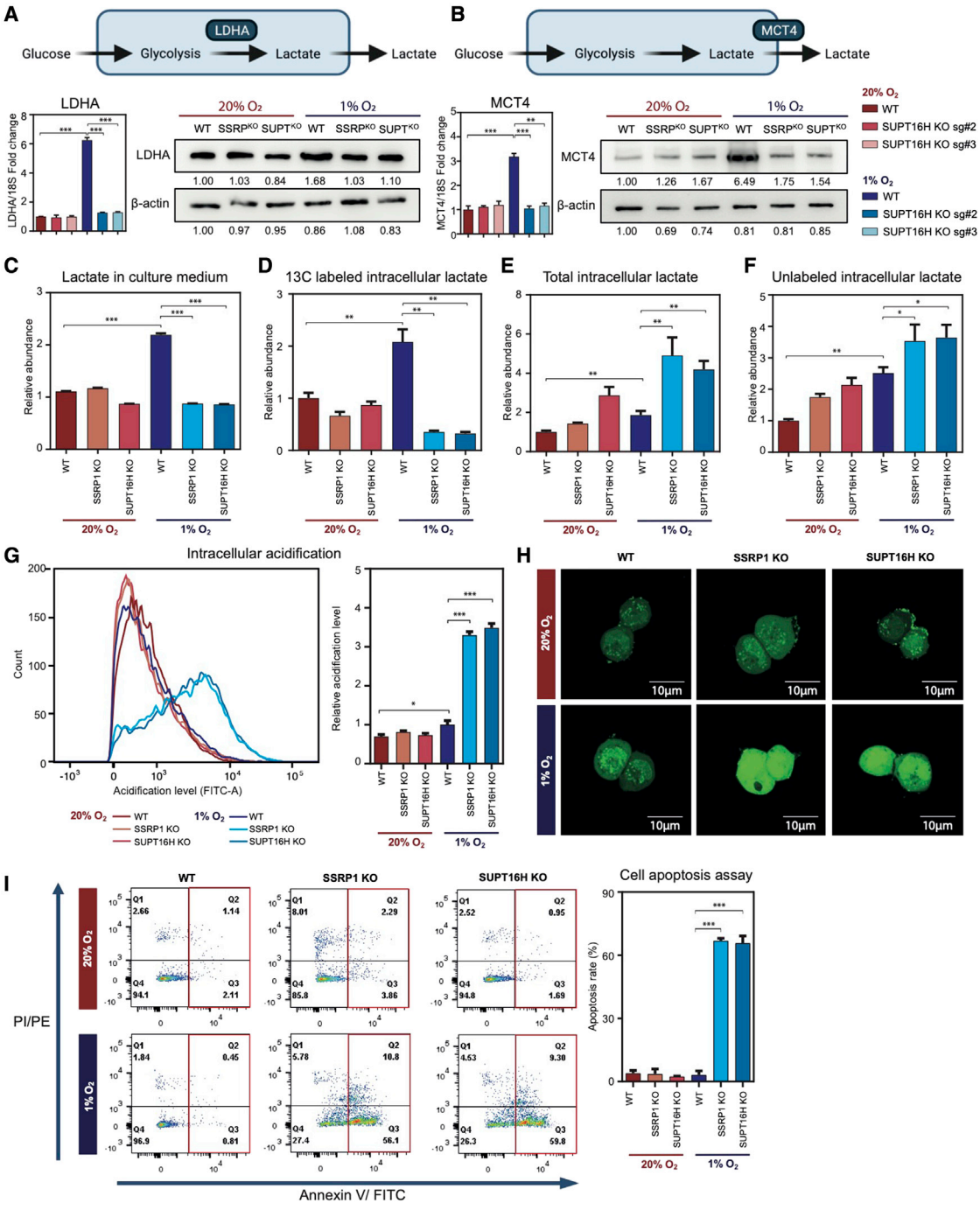

Figure 5. Loss of the FACT complex limits lactate transportation and leads to intracellular acidification

(A and B) Upregulation of lactate dehydrogenase LDHA and lactate transporter MTC4 under hypoxia was validated by qRT-PCR and western blotting. KO of the FACT complex abolished the induction of LDHA (A) and MCT4 (B).

(C) KO of SSRP1 and SUPT16H reduced lactate secretion in culture medium as detected by the colorimetric lactate quantification assay.

(D) Stable isotope tracing with ^{13}C-glucose showed that KO of the FACT complex blocked the hypoxia-induced lactate synthesis in MHCC97L cells.

(E) Total lactate amount in cell lysate was validated by mass spectrometry. KO of the FACT complex led to intracellular lactate accumulation.

(F) The unlabeled lactate (pre-existing lactate) content in the isotope-tracing experiments was validated by mass spectrometry. KO of the FACT complex blocked lactate extrusion in hypoxic condition.

(legend continued on next page)

vital role of the FACT complex in cancer cell growth. Among all common HCC mutations, we observed that the upregulation of the FACT complex was closely associated with TP53 mutations (Figure 6D). We therefore employed a hydrodynamic tail-vein (HDTV) injection approach to simulate the genetic composition of human HCC. HDTV injection delivers a large amount of plasmid solution within 6–8 s into the circulation of the mice, causing temporary cardiac congestion, which mediates the retrograde backflush of plasmids into the liver. The high hydrodynamic pressure compulsorily transfects the liver cells with the genome-editing systems (Figure 6E). Through the HDTV injection approach, we delivered genome-editing systems involving the CRISPR-Cas9 KO system to delete Tp53 and Sleeping Beauty transposon system to overexpress c-Myc, a frequently amplified oncogene in HCC, to induce $Tp53^{KO}$; $c\text{-}Myc^{OE}$ mouse HCC in C57BL/6 mice. Consistent with human HCCs, protein expressions of Ssrp1 and Supt16h were notably overexpressed in mouse HCC induced by HDTV injection (Figure 6F), which further suggests a relationship between the FACT complex upregulation and TP53 mutational status. To further investigate the *in vivo* roles of the FACT complex in HCC initiation, we co-linked sgRNAs targeting Supt16h with sgRNAs targeting Tp53 and found that KO of Supt16h completely hindered the growth of $Tp53^{KO}$; $c\text{-}Myc^{OE}$ HCC (Figures 6E and 6G). To examine the potential clinical benefits of targeting the FACT complex in HCC, we combined current HCC treatment options and the FACT complex inhibition with either genetic KO or small molecular inhibitor curaxin. Clinically, hepatic artery ligation and transcatheter arterial embolization (TAE) are used as common palliative HCC therapies, which restrict HCC tumor growth by limiting blood supply (Wáng et al., 2015). Hepatic artery ligation and TAE inadvertently induce hypoxia and HIFs, which further might promote the aggressiveness of HCC (Sun et al., 2009). We ligated the hepatic artery (Figure 6H) and orthotopically implanted luciferase-labeled MHCC97L-WT, -SSRP1 KO, and -SUPT16H KO cells into the left liver lobe in nude mice. SSRP1 and SUPT16H KO tumors could only be barely formed in livers with hepatic ligation, and lung metastasis was curbed by KO of SSRP1 and SUPT16H (Figures 6I–6K; Figure S7E). The FACT complex inhibitor curaxin also showed a similar effect by inhibiting tumorigenesis and lung metastasis upon hepatic artery ligation (Figures S7A and S7B). H&E staining confirmed the formation of lung metastasis, enhanced cancer cell proliferation, and angiogenesis in DMSO-treated mice, but not in the curaxin-treated group (Figures S7C and S7D). Besides hepatic artery ligation, current U.S. Food and Drug Administration (FDA)-approved targeted therapies in HCC, including bevacizumab, sorafenib, lenvatinib, and cabozantinib, are all inhibiting the VEGF signaling. As VEGF can induce angiogenesis, anti-VEGF therapies resulted in intratumoral hypoxia and activation of HIFs (Miyazaki et al., 2014). Given the critical roles of the FACT complex in hypoxic response, we asked whether inhibition of the FACT complex would further hinder the growth of HCC by blocking the transcription of hypoxic genes. To this end, we tested combined therapies of the FACT complex inhibitor curaxin and a VEGF antibody drug bevacizumab. Results showed that curaxin and bevacizumab co-treatment exhibited a more potent effect in suppressing HCC tumor growth and lung metastasis in an orthotopic implantation model (Figures 7A–7D). Single treatment with curaxin or bevacizumab significantly suppressed tumor growth, while their co-treatment almost completely blocked tumorigenesis. Immunohistochemistry (IHC) staining also confirmed that co-treatment with both drugs showed a synergistic effect on inhibition of proliferation (KI67) as well as angiogenesis (CD31; Figures 7E and 7F). Moreover, curaxin and bevacizumab treatments are well tolerated in mice (Figure 7G), highlighting the translational value of this new therapeutic combination for HCC patients. Previously, we reported curaxin sensitized the anti-tumor effects of the first-line HCC drug sorafenib. Similar effects were also observed upon co-treatment with curaxin and other HCC drugs, lenvatinib and cabozantinib (Figures S7F–S7J). We reasoned that the synergistic anti-tumor effects in combined therapies were due to the critical roles of the FACT complex in hypoxia response. Treatment with bevacizumab, lenvatinib, sorafenib, and cabozantinib induced the expression of hypoxia response genes in *in vivo* orthotopically implanted tumors, while co-treatment with curaxin significantly abolished the hypoxia-induced CA9, GLUT1, LOX, and VEGFA expressions (Figure 7H). Consequently, inhibition of the FACT complex created a vulnerability toward hypoxic stress that amplified the anti-cancer effect of anti-angiogenetic therapies. Therefore, co-treatment with the FACT complex inhibitor curaxin remarkably hinders the growth of the hypoxic tumors in above-mentioned HCC models. Collectively, our findings suggested that the histone chaperone FACT complex mediates metabolic adaptation to hypoxic stress in cancer. Our results also exemplified an effective therapeutic approach by targeting the FACT complex for cancer patients.

DISCUSSION

The histone chaperone FACT complex was frequently upregulated in various cancers (Barone et al., 2017; Carter et al., 2015b; Garcia et al., 2013; Shen et al., 2020). However, studies on the oncogenic and biological functions of histone chaperones are still limited, and the molecular mechanisms by which its histone traffic and nucleosome dynamics contribute to cancer development are waiting to be elucidated. In this study, we found that the FACT complex mediates transcription elongation of hypoxia-response genes, thereby allowing a rapid cellular adaptation to hypoxic stress. Moreover, the histone chaperone FACT complex represents an enticing therapeutic target in hypoxic cancers.

(G and H) Intracellular acidification level was indicated by an intracellular pH indicator followed by flow cytometry analysis (G) and live-cell imaging (H). The FACT-complex-depleted cells cultured in hypoxia showed significant acidification compared with WT cells. FITC, fluorescein isothiocyanate.
(I) Hypoxia induced apoptosis in SSRP1 and SUPT16H KO cells as detected by annexin V/phosphatidylinositol (PI) staining.
(A–G and I) Data represent the mean ± SD from triplicate experiments. *$p < 0.05$; **$p < 0.01$; ***$p < 0.001$; Student's t test. (A and B) Quantification of protein expressions was performed by Image Lab software v.6.1. See also Figure S5.

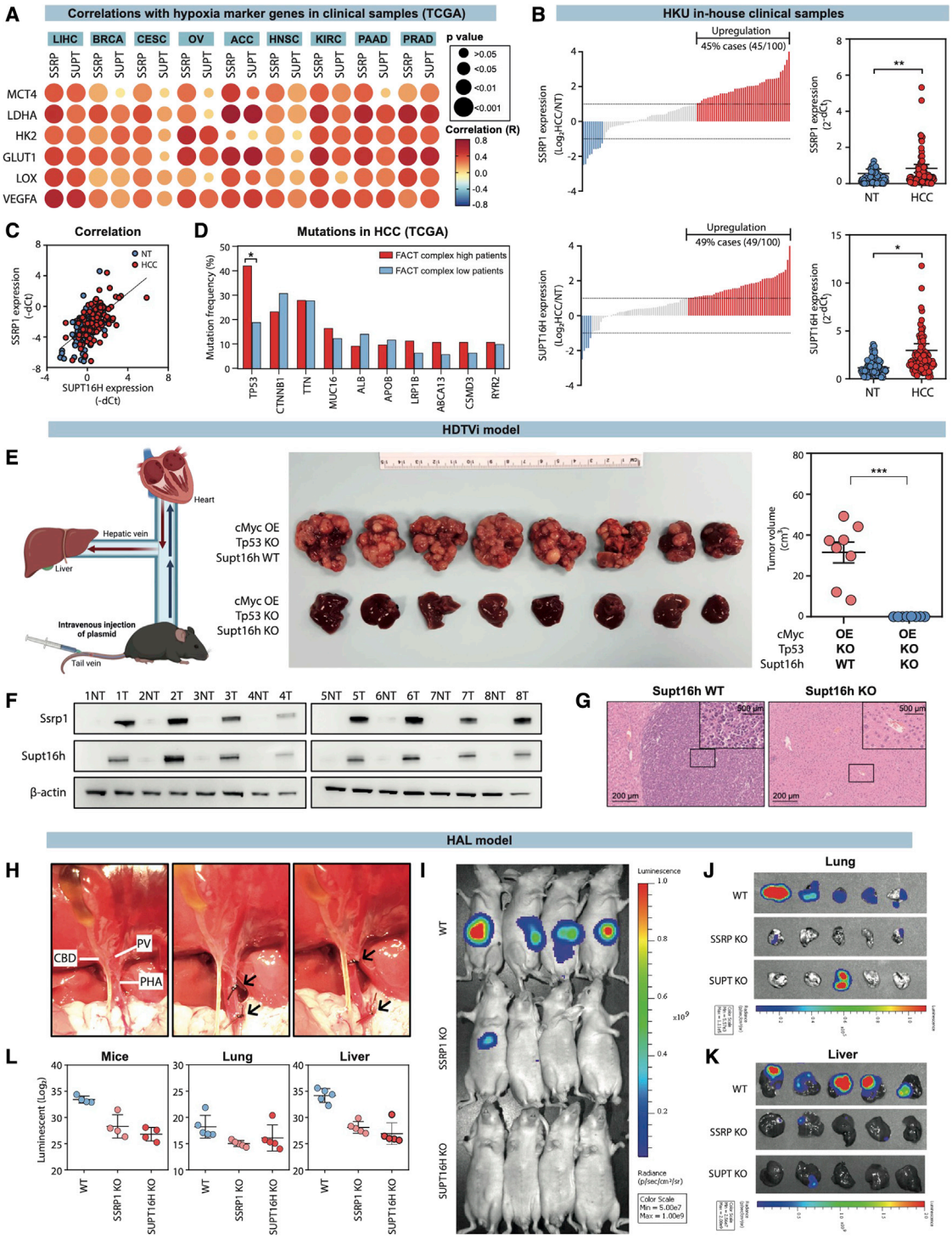

Figure 6. The FACT complex plays a role during tumor initiation and progression in liver cancer

(A) Correlations between the FACT complex and hypoxia-induced genes in clinical cancer samples from the TCGA cohorts were indicated according to sample correlation coefficient (R) and the corresponding p values. The expressions of SSRP1 and SUPT16H and VEGFA, LOX, GLUT1, HK2, LDHA, and MCT4 were significantly correlated in multiple human cancers. Genes with $R > 0.4$ are considered well correlated, and $p < 0.05$ is regarded as statically significant. ACC, adrenocortical carcinoma; BRCA, breast invasive carcinoma; CESC, cervical squamous cell carcinoma and endocervical adenocarcinoma; HNSC, head and neck squamous cell carcinoma; KIRC, kidney renal clear cell carcinoma; LIHC, liver hepatocellular carcinoma; OV, ovarian serous cystadenocarcinoma; PAAD, pancreatic adenocarcinoma; PRAD, prostate adenocarcinoma.

(legend continued on next page)

To support continuous growth in the challenging hypoxic environment, cancer cells are found to alter their transcription program to adapt to hypoxic stress. Past studies have focused on the discovery of mechanisms that identified transcriptional cofactors that support HIF-1 transcriptional activity. Under normoxia, HIF-1α is hydroxylated and ubiquitinated through PHD/VHL axis. Under hypoxia, HIF-1α is stabilized and dimerizes with HIF-1β, together with other co-activators, such as CBP and P300 (Arany et al., 1996), to activate transcription initiation (Wang et al., 1995). These findings aim at understanding the contributing factors that facilitate the transcription initiation by HIF-1, the first step of transcription. Transcription elongation, which is as important as transcription initiation to control the transcriptional program in hypoxic cells, has never been clearly elucidated. Herein, we demonstrated that the histone chaperone FACT complex is actively involved in supporting the elongation of HIF-mediated transcription. The FACT complex has two subunits, SSRP1 and SUPT16H (Wittmeyer et al., 1999). When a transcribing polymerase approaches, SSRP1 binds to H3-H4 histones and SUPT16H removes H2A-H2B histones from the nucleosome to facilitate the passage of RNA polymerase II (Saunders et al., 2003). This unique function of the FACT complex in facilitating nucleosome disassembly and reassembly supports a rapid passage of RNA Pol II for overcoming individual nucleosome barriers. Therefore, upregulation of the FACT complex allows hypoxic cancer cells to induce a transcriptional program through HIF-1 to promptly adapt to low oxygen conditions.

Besides transcriptional control, translation mechanisms that mediate hydroxylation and degradation of HIF proteins ensure an adaptive mechanism to favor hypoxic cells. In the presence of O_2, the proline residues 402 and 564 of HIF-1α are hydroxylated by PHDs (Epstein et al., 2001). Prolyl-hydroxylated HIF-1α is recognized by VHL, which mediates ubiquitination and proteasomal degradation of HIF-1α (Kaelin and Ratcliffe, 2008). Our study showed that the FACT complex is regulated by PHD/VHL axis in a similar manner. However, unlike HIF-1α, which is mostly degraded in the presence of O_2, SSRP1 and SUPT16H proteins are still detectable in normoxic condition. The stabilization of the FACT complex by hypoxia is not as dramatic as HIF-1α. This is consistent with the understanding that the FACT complex is responsible for transcription elongation in other contexts. Another possible explanation is that the FACT complex is regulated by various E3 ligases. A yeast study shows that SUPT16H homolog in yeast was regulated by an E3 ligase San1 and Rtt101 (Han et al., 2010; Sen et al., 2016). In our previous findings, we also showed that the FACT complex is modified by E3 ligase KEAP1 and mediates NRF2-mediated oxidative stress response. We therefore speculated that such degradation mechanisms of the FACT complex enable the cells to quickly coordinate with the corresponding transcription factors to drive the transcription programs in different cellular stresses.

Transcriptional and translational regulatory mechanisms allow HIF-1 to assist cells to adapt by activating genes that favor glycolysis and reduce oxidative phosphorylation (Semenza, 2012). One of the transcriptional targets allowing HIF-1 to divert metabolites into glycolysis instead of oxidative phosphorylation is LDHA (Semenza et al., 1996). LDHA converts pyruvate into lactate, preventing pyruvate from being converted into acetyl-CoA, which otherwise enters the TCA cycle. To prevent intracellular acidification, HIF-1 also induces the transcription of MCT4, which extrudes lactate (Sonveaux et al., 2008). In this study, transcriptome sequencing and ^{13}C metabolic flux analysis clearly demonstrated that hypoxic cancer cells could not completely switch to glycolysis when the FACT complex was knocked out. Interestingly, intracellular lactate was accumulated in hypoxic cancer cells when the FACT complex was knocked out, eventually causing intracellular acidification and apoptosis. Our current study focuses on the metabolic rewiring known to be driven by HIF-1. However, transcriptome sequencing data in the FACT complex KO HCC cells clearly indicated that the FACT complex also regulates other HIF-1 transcriptional targets responsible for many different phenotypes, such as angiogenesis (VEGFA), intravasation and extravasation (ANGPTL4), extracellular matrix (ECM) modification (LOX), metabolic rewiring (NDUFA4L2), and pH homeostasis (CA9). Considering HIF-1 has versatile roles in cancer development by transcriptionally activating a broad spectrum of genes, including genes involved in promoting chemo-resistance, cancer stemness, angiogenesis, epithelial-mesenchymal transition, metastasis, ECM modifications, and immune evasion (Schito and Semenza, 2016; Yuen and Wong, 2020), the FACT complex might also play imperative roles in almost every step of oncogenesis driven by HIF-1. However, oxygen depletion elicits both acute and chronic response in cancer cells. Considering the essential role of the FACT complex during

(B) mRNA expressions of SSRP1 and SUPT16H were determined by qRT-PCR in 100 pairs of human HCC and their corresponding non-tumorous (NT) liver tissues. Waterfall plot shows that SSRP1 was upregulated in 45% and SUPT16H was overexpressed in 49% of HCC patients by at least 2-fold.
(C) Expressions of SSRP1 and SUPT16H were significantly correlated in human HCC and NT liver samples.
(D) Correlation between HCC common mutations and the FACT complex expression status. TP53 mutation was more frequently found in HCC patients with high FACT complex expression.
(E) Role of the FACT complex during HCC initiation was demonstrated by a hydrodynamic tail vein (HDTV) injection model (n = 8 in each group). KO of Supt16h abolished $Tp53^{KO}$-$cMyc^{OE}$-induced HCC formation.
(F) Western blot confirmed the significant increase of Ssrp1 and Supt16h in $Tp53^{KO}$ $cMyc^{OE}$ tumors when compared with corresponding normal livers.
(G) H&E staining confirmed the formation of HCC upon $Tp53^{KO}$ and $cMyc^{OE}$.
(H) Surgical procedures of hepatic artery ligation. The common hepatic artery was ligated with two silk sutures and excised in the middle. CBD, common bile duct; PHA, proper hepatic artery; PV, portal vein.
(I–L) 2×10^6 WT (n = 5), SSRP1 KO (n = 5), and SUPT16H KO (n = 5) luc + MHCC97L cells were orthotopically injected into the liver of BALB/c nude mice with hepatic artery ligated. Bioluminescence of (I) mice, (J) lung metastasis, and (K) orthotopic tumors formed in livers was recorded and plotted in (L). Tumor size was calculated based on bioluminescence.
(B) Data represent the mean ± SD of 100 patient samples. (E and L) Error bar indicates the mean ± SD from each mice group. Data represent the mean ± SD from triplicate experiments. *$p < 0.05$; **$p < 0.01$; ***$p < 0.001$; Student's t test. See also Figure S6.

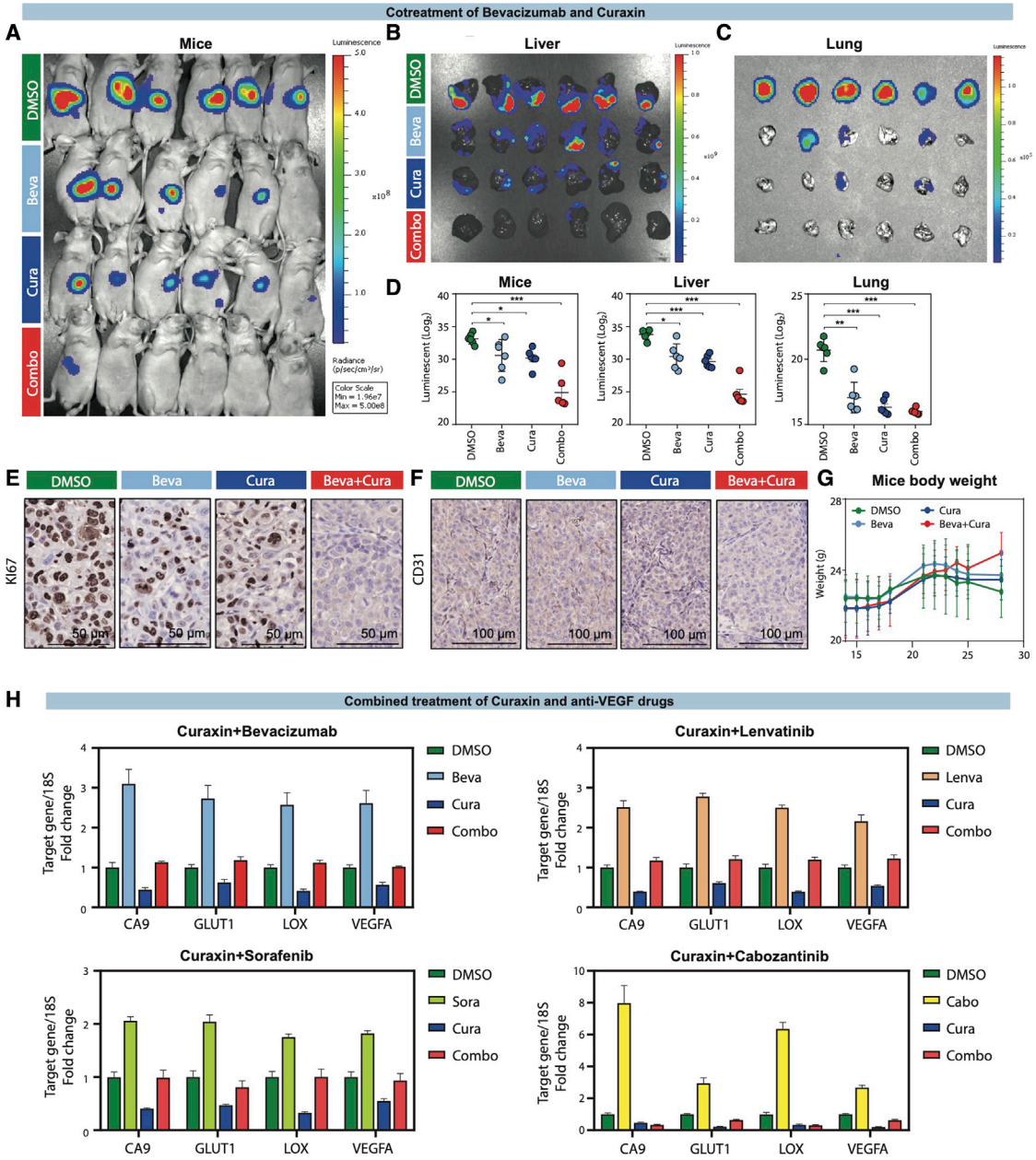

Figure 7. Targeting the FACT complex sensitizes the anti-tumor effects of anti-angiogenic drugs in liver cancer

(A–D) 2 × 10^6 luciferase-labeled MHCC97L was implanted into left liver lobes of male BALB/c nude mice by orthotopic injection. Tumors were allowed to grow for 2 weeks and then tumor-bearing mice were subjected to (1) vehicle (n = 6), (2) 15 mg/kg curaxin by oral gavage on a 5-days-on/2-days-off schedule (n = 6), (3) 1 mg/kg bevacizumab by tail-vein injection twice per week (n = 6), or (4) co-treatment of curaxin and bevacizumab (n = 6). Mice in the co-treatment (combo) group had significantly reduced tumor size and lung metastasis when compared with single treatments. Data are as calculated based on bioluminescent imaging (A–D).

(E and F) Immunohistochemistry staining of HCC tumors from DMSO, bevacizumab, curaxin, and bevacizumab and curaxin co-treated mice with KI67 (E) and CD31 (F) antibodies.

(G) Body weights of mice.

(H) Curaxin treatment inhibited the increase of hypoxia-inducible genes CA9, GLUT1, LOX, and VEGFA in *in vivo* tumor xenografts treated with bevacizumab, lenvatinib, sorafenib, and cabozantinib.

(D and G) Error bar indicates mean ± SD from each mice group (n = 6). (H) Data represent the mean ± SD from triplicate experiments. *p < 0.05; **p < 0.01; ***p < 0.001; Student's t test. See also Figure S7.

transcription elongation, we mainly focused on rapid-onset steps driven by HIF-1 in this study, while the FACT complex and HIFs might regulate differentially on some long-term responses during hypoxia adaptation.

Besides hypoxic stress, cancer cells have higher capability to overcome different types of stresses by triggering stress response systems expeditiously to maintain a homeostatic balance to survive. Stress response involves the activation of different transcriptional programs for the cellular adaptations to specific types of stress. Heat-shock response (HSR), unfolded protein response (UPR), oxidative stress response, and hypoxia response are the most common and widely studied stress responses that are governed by specific transcription factors (Himanen and Sistonen, 2019). Heat shock results in cytoplasmic protein aggregation, inducing the trimerization of transcription factor subunits HSF1 and HSF2 to initiate transcription of genes involved in protein folding and clearance of protein aggregates. Meanwhile, heat shock also activates serum response factor (SRF) to initiate transcription of heat-induced cytoskeletal genes (Mahat et al., 2016). ER stress, resulting from overload of unfolded proteins at ER, activates the UPR, which comprises the three pathways governed by IRE1, PERK, and ATF6 to resolve unfolded proteins (Almanza et al., 2019). Oxidative stress, as a result of over-production of reactive oxygen species (ROS), releases NRF2 from KEAP1 binding and KEAP1-mediated ubiquitination and subsequent proteasomal degradation so that stabilized NRF2 and NRF2 translocated into the nucleus to initiate transcription of genes involved in antioxidant response (Dhakshinamoorthy et al., 2005; Keum, 2011). During hypoxia, PHDs could no longer hydroxylate HIF-1/2α and be recognized by VHL protein, which otherwise subjects HIF-1/2α for ubiquitin-mediated protein degradation (Kaelin and Ratcliffe, 2008). HIF-1/2α is stabilized and dimerizes with HIF-1β to mediate transcription of genes that allow cells to adapt to low O_2 content. In this study, we demonstrated the important role of the FACT complex in mediating hypoxia adaptation. Previously, we also showed that FACT complex plays a role in response to oxidative stress. Noteworthily, the FACT complex is a transcriptional target of NRF2, the master regulator of antioxidative responses, and that the FACT complex facilitates the transcription elongation of NRF2 as well as NRF2 transcriptional targets responsible for antioxidant production, reinforcing the feedforward loop to amplify the transcriptional programs for antioxidant genes. However, our transcriptome sequencing data and *in silico* analysis of the FACT promoter for HIF-consensus binding site or hypoxia response element (HRE) showed that the FACT complex is not a transcriptional target of HIF-1/2. We surmise that the detailed interaction and regulatory mechanisms of FACT complex and the key transcription factors (TFs) in different types of stress response might be slightly different, meriting further explorations. The FACT complex mediates prompt nucleosome disassembly to expedite the passage of RNA Pol II to support transcription elongation. We therefore speculate that FACT complex might also play important roles in the transcription elongation of genes involved in HSR and UPR. Interestingly, HSF1 through binding with replication protein A (RPA) has been shown to facilitate RNA Pol II loading and recruit the FACT complex to promoter of HSP70 (Fujimoto et al., 2012). Although this study did not provide evidence with regards to the roles of the FACT complex in HSF1-mediated transcriptional elongation, it clearly highlighted that the FACT complex might also be involved in HSR. To conclude, our study exemplified the crucial roles of the FACT complex in hypoxia response in cancer cells and highlighted the connection between metabolic and transcriptional regulation in carcinogenesis.

Limitations of the study

How cancer cells respond to environmental and biological stress remains a central question of cancer biology. Herein, we used SSRP1/SUPT16H KO clones and a small molecular inhibitor, curaxin, to demonstrate the essential role of the histone chaperone FACT complex during hypoxia adaptation. In this study, we mainly focus on the implications of the FACT complex in HIF-mediated metabolic reprogramming in cancer cells. Further studies are needed to establish the versatile roles of the histone chaperone FACT complex in other HIF-mediated pathways.

STAR★METHODS

Detailed methods are provided in the online version of this paper and include the following:

- KEY RESOURCES TABLE
- RESOURCE AVAILABILITY
  - Lead contact
  - Materials availability
  - Data and code availability
- EXPERIMENTAL MODEL AND SUBJECT DETAILS
  - Patient samples and cell lines
  - Establishment of the FACT complex and VHL knockout cells
  - Orthotopic liver implantation and hepatic artery ligation mice models
  - *In vivo* drug treatment on mice models
  - Hydrodynamic tail vein (HDTV) injection mice models
- METHOD DETAILS
  - Knockdown of PHD1-3, HIF1A/HIF2A by siRNAs
  - Transcriptome sequencing and pathway analysis
  - Cell viability, proliferation, migration assay and colony formation assay
  - Reverse transcription quantitative PCR (RT-qPCR)
  - Protein extraction and Western blot
  - Intracellular pH detection
  - Glucose uptake assay
  - Lactate production
  - GC/MS metabolites profiling
  - LC-MS/MS hydroxyproline site detection
  - Cell apoptosis assay
  - Transcription elongation assay
  - Polyubiquitin pull-down assay
  - Immunoprecipitation of prolyl-hydroxylated proteins
  - Immunohistochemistry
  - Orthotopic liver implantation and hepatic artery ligation model
  - *In vivo* drug treatment

- Hydrodynamic tail vein (HDTV) injection model
- Chemicals and drug dilution

- QUANTIFICATION AND STATISTICAL ANALYSIS

SUPPLEMENTAL INFORMATION

Supplemental information can be found online at https://doi.org/10.1016/j.celrep.2022.110304.

ACKNOWLEDGMENTS

We thank Dr. Clive Chung for his advice in the hydroxylation profiling study. We thank the Core Facility, Center for Genomic Sciences and Proteomics and Metabolomics Core of LKS Faculty of Medicine for their technical support in Sanger sequencing, flow cytometry analyses, Xenogen imaging, live-cell imaging, and LC-MS/MS measurements. We also thank the Laboratory Animal Unit for animal housing. The study was supported by HMRF (05161786), RGC-GRF (17108720), and RGC-TBRS (T12-704/16-R). C.C.-L.W. received fundings from the Croucher Foundation (Croucher Innovation Award) and the University of Hong Kong (HKU Outstanding Young Researcher Award).

AUTHOR CONTRIBUTIONS

Conceptualization, J.S., C.C.-L.W., and C.-M.W.; methodology, J.S., C.C.-L.W., and C.-M.W.; formal analysis, J.S., C.-T.L., G.W., and C.-M.W.; investigation, J.S., C.Y., M.S.Z., D.W.-C.C., F.-F.C., C.L.-H.C., M.C., R.T.-C.W., M.W., Z.K., R.S., T.K.W.L., C.C.-L.W., and C.-M.W.; resource, I.O.-L.N., C.C.-L.W., and C.-M.W.; funding acquisition, I.O.-L.N., C.C.-L.W., and C.-M.W.; writing – original draft, J.S., C.C.-L.W., and C.-M.W.; writing – review and editing, J.S., C.C.-L.W., and C.-M.W.; supervision, C.C.-L.W. and C.-M.W.

DECLARATION OF INTERESTS

The authors declare no competing interests.

Received: December 7, 2020
Revised: November 16, 2021
Accepted: January 5, 2022
Published: February 1, 2022

REFERENCES

Almanza, A., Carlesso, A., Chintha, C., Creedican, S., Doultsinos, D., Leuzzi, B., Luís, A., McCarthy, N., Montibeller, L., More, S., et al. (2019). Endoplasmic reticulum stress signalling - from basic mechanisms to clinical applications. FEBS J. *286*, 241–278.

Antoniewicz, M.R., Kelleher, J.K., and Stephanopoulos, G. (2007). Accurate assessment of amino acid mass isotopomer distributions for metabolic flux analysis. Anal. Chem. *79*, 7554–7559.

Arany, Z., Huang, L.E., Eckner, R., Bhattacharya, S., Jiang, C., Goldberg, M.A., Bunn, H.F., and Livingston, D.M. (1996). An essential role for p300/CBP in the cellular response to hypoxia. Proc. Natl. Acad. Sci. U S A *93*, 12969–12973.

Barone, T.A., Burkhart, C.A., Safina, A., Haderski, G., Gurova, K.V., Purmal, A.A., Gudkov, A.V., and Plunkett, R.J. (2017). Anticancer drug candidate CBL0137, which inhibits histone chaperone FACT, is efficacious in preclinical orthotopic models of temozolomide-responsive and -resistant glioblastoma. Neuro Oncol. *19*, 186–196.

Belotserkovskaya, R., Oh, S., Bondarenko, V.A., Orphanides, G., Studitsky, V.M., and Reinberg, D. (2003). FACT facilitates transcription-dependent nucleosome alteration. Science *301*, 1090–1093.

Carrozza, M.J., Kusch, T., and Workman, J.L. (2003). Repairing nucleosomes during transcription. Nat. Struct. Biol. *10*, 879–880.

Carter, D.R., Murray, J., Cheung, B.B., Gamble, L., Koach, J., Tsang, J., Sutton, S., Kalla, H., Syed, S., Gifford, A.J., et al. (2015a). Therapeutic targeting of the MYC signal by inhibition of histone chaperone FACT in neuroblastoma. Sci. Transl. Med. *7*, 312ra176.

Carter, D.R., Murray, J., Cheung, B.B., Gamble, L., Koach, J., Tsang, J., Sutton, S., Kalla, H., Syed, S., Gifford, A.J., et al. (2015b). Therapeutic targeting of the MYC signal by inhibition of histone chaperone FACT in neuroblastoma. Sci. Transl. Med. *7*, 312ra176.

Chen, C., Pore, N., Behrooz, A., Ismail-Beigi, F., and Maity, A. (2001). Regulation of glut1 mRNA by hypoxia-inducible factor-1. Interaction between H-ras and hypoxia. J. Biol. Chem. *276*, 9519–9525.

Dhakshinamoorthy, S., Jain, A.K., Bloom, D.A., and Jaiswal, A.K. (2005). Bach1 competes with Nrf2 leading to negative regulation of the antioxidant response element (ARE)-mediated NAD(P)H:quinone oxidoreductase 1 gene expression and induction in response to antioxidants. J. Biol. Chem. *280*, 16891–16900.

Epstein, A.C., Gleadle, J.M., McNeill, L.A., Hewitson, K.S., O'Rourke, J., Mole, D.R., Mukherji, M., Metzen, E., Wilson, M.I., Dhanda, A., et al. (2001). C. elegans EGL-9 and mammalian homologs define a family of dioxygenases that regulate HIF by prolyl hydroxylation. Cell *107*, 43–54.

Fuchs, G., Voichek, Y., Rabani, M., Benjamin, S., Gilad, S., Amit, I., and Oren, M. (2015). Simultaneous measurement of genome-wide transcription elongation speeds and rates of RNA polymerase II transition into active elongation with 4sUDRB-seq. Nat. Protoc. *10*, 605–618.

Fujimoto, M., Takaki, E., Takii, R., Tan, K., Prakasam, R., Hayashida, N., Iemura, S., Natsume, T., and Nakai, A. (2012). RPA assists HSF1 access to nucleosomal DNA by recruiting histone chaperone FACT. Mol. Cell *48*, 182–194.

Garcia, H., Fleyshman, D., Kolesnikova, K., Safina, A., Commane, M., Paszkiewicz, G., Omelian, A., Morrison, C., and Gurova, K. (2011). Expression of FACT in mammalian tissues suggests its role in maintaining of undifferentiated state of cells. Oncotarget *2*, 783–796.

Garcia, H., Miecznikowski, J.C., Safina, A., Commane, M., Ruusulehto, A., Kilpinen, S., Leach, R.W., Attwood, K., Li, Y., Degan, S., et al. (2013). Facilitates chromatin transcription complex is an "accelerator" of tumor transformation and potential marker and target of aggressive cancers. Cell Rep. *4*, 159–173.

Gasparian, A.V., Burkhart, C.A., Purmal, A.A., Brodsky, L., Pal, M., Saranadasa, M., Bosykh, D.A., Commane, M., Guryanova, O.A., Pal, S., et al. (2011). Curaxins: anticancer compounds that simultaneously suppress NF-kappaB and activate p53 by targeting FACT. Sci. Transl. Med. *3*, 95ra74.

Han, J., Li, Q., McCullough, L., Kettelkamp, C., Formosa, T., and Zhang, Z. (2010). Ubiquitylation of FACT by the cullin-E3 ligase Rtt101 connects FACT to DNA replication. Genes Dev. *24*, 1485–1490.

Himanen, S.V., and Sistonen, L. (2019). New insights into transcriptional reprogramming during cellular stress. J. Cell Sci. *132*, jcs238402.

Kaelin, W.G., and Ratcliffe, P.J. (2008). Oxygen sensing by metazoans: the central role of the HIF hydroxylase pathway. Mol. Cell *30*, 393–402.

Keum, Y.S. (2011). Regulation of the Keap1/Nrf2 system by chemopreventive sulforaphane: implications of posttranslational modifications. Ann. N. Y. Acad. Sci. *1229*, 184–189.

Lopez, Y., Nakai, K., and Patil, A. (2015). HitPredict version 4: comprehensive reliability scoring of physical protein-protein interactions from more than 100 species. Database (Oxford) *2015*, bav117.

Mahat, D.B., Salamanca, H.H., Duarte, F.M., Danko, C.G., and Lis, J.T. (2016). Mammalian heat shock response and mechanisms Underlying its genome-wide transcriptional regulation. Mol. Cell *62*, 63–78.

Miyazaki, S., Kikuchi, H., Iino, I., Uehara, T., Setoguchi, T., Fujita, T., Hiramatsu, Y., Ohta, M., Kamiya, K., Kitagawa, K., et al. (2014). Anti-VEGF antibody therapy induces tumor hypoxia and stanniocalcin 2 expression and potentiates growth of human colon cancer xenografts. Int. J. Cancer *135*, 295–307.

Orphanides, G., Wu, W.H., Lane, W.S., Hampsey, M., and Reinberg, D. (1999). The chromatin-specific transcription elongation factor FACT comprises human SPT16 and SSRP1 proteins. Nature *400*, 284–288.

Park, H.J., Lyons, J.C., Ohtsubo, T., and Song, C.W. (1999). Acidic environment causes apoptosis by increasing caspase activity. Br. J. Cancer *80*, 1892–1897.

Royer, C., Lachuer, J., Crouzoulon, G., Roux, J., Peyronnet, J., Mamet, J., Pequignot, J., and Dalmaz, Y. (2000). Effects of gestational hypoxia on mRNA levels of Glut3 and Glut4 transporters, hypoxia inducible factor-1 and thyroid hormone receptors in developing rat brain. Brain Res. *856*, 119–128.

Saunders, A., Werner, J., Andrulis, E.D., Nakayama, T., Hirose, S., Reinberg, D., and Lis, J.T. (2003). Tracking FACT and the RNA polymerase II elongation complex through chromatin in vivo. Science *301*, 1094–1096.

Schito, L., and Semenza, G.L. (2016). Hypoxia-inducible factors: master regulators of cancer progression. Trends Cancer *2*, 758–770.

Semenza, G.L. (2001). HIF-1, O(2), and the 3 PHDs: how animal cells signal hypoxia to the nucleus. Cell *107*, 1–3.

Semenza, G.L. (2012). Hypoxia-inducible factors in physiology and medicine. Cell *148*, 399–408.

Semenza, G.L., Jiang, B.H., Leung, S.W., Passantino, R., Concordet, J.P., Maire, P., and Giallongo, A. (1996). Hypoxia response elements in the aldolase A, enolase 1, and lactate dehydrogenase A gene promoters contain essential binding sites for hypoxia-inducible factor 1. J. Biol. Chem. *271*, 32529–32537.

Sen, R., Ferdoush, J., Kaja, A., and Bhaumik, S.R. (2016). Fine-tuning of FACT by the ubiquitin proteasome system in regulation of transcriptional elongation. Mol. Cell Biol. *36*, 1691–1703.

Shen, J., Chen, M., Lee, D., Law, C.T., Wei, L., Tsang, F.H., Chin, D.W., Cheng, C.L., Lee, J.M., Ng, I.O., et al. (2020). Histone chaperone FACT complex mediates oxidative stress response to promote liver cancer progression. Gut *69*, 329–342.

Sonveaux, P., Vegran, F., Schroeder, T., Wergin, M.C., Verrax, J., Rabbani, Z.N., De Saedeleer, C.J., Kennedy, K.M., Diepart, C., Jordan, B.F., et al. (2008). Targeting lactate-fueled respiration selectively kills hypoxic tumor cells in mice. J. Clin. Invest. *118*, 3930–3942.

Sun, X., Jiang, H., Jiang, X., Tan, H., Meng, Q., Sun, B., Xu, R., and Krissansen, G.W. (2009). Antisense hypoxia-inducible factor-1alpha augments transcatheter arterial embolization in the treatment of hepatocellular carcinomas in rats. Hum. Gene Ther. *20*, 314–324.

Todenhöfer, T., Seiler, R., Stewart, C., Moskalev, I., Gao, J., Ladhar, S., Kamjabi, A., Al Nakouzi, N., Hayashi, T., Choi, S., et al. (2018). Selective inhibition of the lactate transporter MCT4 reduces growth of invasive bladder cancer. Mol. Cancer Ther. *17*, 2746–2755.

Ullah, M.S., Davies, A.J., and Halestrap, A.P. (2006). The plasma membrane lactate transporter MCT4, but not MCT1, is up-regulated by hypoxia through a HIF-1alpha-dependent mechanism. J. Biol. Chem. *281*, 9030–9037.

Wang, G.L., Jiang, B.H., Rue, E.A., and Semenza, G.L. (1995). Hypoxia-inducible factor 1 is a basic-helix-loop-helix-PAS heterodimer regulated by cellular O2 tension. Proc. Natl. Acad. Sci. U S A *92*, 5510–5514.

Wang, V., Davis, D.A., Haque, M., Huang, L.E., and Yarchoan, R. (2005). Differential gene up-regulation by hypoxia-inducible factor-1alpha and hypoxia-inducible factor-2alpha in HEK293T cells. Cancer Res. *65*, 3299–3306.

Wáng, Y.X., De Baere, T., Idée, J.M., and Ballet, S. (2015). Transcatheter embolization therapy in liver cancer: an update of clinical evidences. Chin. J. Cancer Res. *27*, 96–121.

Wittmeyer, J., Joss, L., and Formosa, T. (1999). Spt16 and Pob3 of Saccharomyces cerevisiae form an essential, abundant heterodimer that is nuclear, chromatin-associated, and copurifies with DNA polymerase alpha. Biochemistry *38*, 8961–8971.

Yoon, D.Y., Buchler, P., Saarikoski, S.T., Hines, O.J., Reber, H.A., and Hankinson, O. (2001). Identification of genes differentially induced by hypoxia in pancreatic cancer cells. Biochem. Biophys. Res. Commun. *288*, 882–886.

Yuen, V.W., and Wong, C.C. (2020). Hypoxia-inducible factors and innate immunity in liver cancer. J. Clin. Invest. *130*, 5052–5062.

STAR★METHODS

KEY RESOURCES TABLE

REAGENT or RESOURCE	SOURCE	IDENTIFIER
Antibodies		
Rabbit Polyclonal antibody anti-SUPT16H	Abcam	Cat#ab204343
Mouse Polyclonal antibody anti-GLUT1	Abcam	Cat#ab15309; RRID:AB_301844
Rabbit Polyclonal antibody anti-Hydroxyproline	Abcam	Cat#ab37067; RRID:AB_873885
Recombinant Anti-Ki67 antibody [SP6]	Abcam	Cat#ab16667; RRID:AB_302459
Rabbit Monoclonal antibody anti-SSRP1 (E1Y8D)	Cell Signaling Technology	Cat#13412
Rabbit Polyclonal antibody anti-β-actin	Cell Signaling Technology	Cat#4967; RRID:AB_330288
Rabbit Polyclonal antibody anti-HIF1α	Cell Signaling Technology	Cat#3716S; RRID:AB_2116962
Mouse Polyclonal antibody anti-VHL	Cell Signaling Technology	Cat#68547S; RRID:AB_2716279
Mouse Monocloncal antibody anti-GLUT3 (G-5)	Santa Cruz	sc-74399; RRID:AB_1124975
Mouse Monocloncal antibody anti-GPI (H-10)	Santa Cruz	sc-365066; RRID:AB_10841426
Mouse Monocloncal antibody anti-HK2 (B-8)	Santa Cruz	sc-374091; RRID:AB_10917915
Mouse Monocloncal antibody anti-MCT4 (D-1)	Santa Cruz	sc-376140; RRID:AB_10992036
Mouse Monocloncal antibody anti-LDHA (E-9)	Santa Cruz	sc-137243; RRID:AB_2137192
Mouse Monocloncal antibody anti-Aldolase C (H-11)	Santa Cruz	sc-271593; RRID:AB_10659113
Mouse Monocloncal antibody anti-PKM (C-11)	Santa Cruz	sc-365684; RRID:AB_10844484
Normal rabbit IgG polyclonal antibody control	Millipore	12-370; RRID:AB_145841
Normal mouse IgG polyclonal antibody control	Millipore	12-371; RRID:AB_145840
CD31/PECAM-1 rabbit polyclonal antibody	ThermoFisher	Cat#RB10333; RRID:AB_720501
Chemicals, peptides, and recombinant proteins		
HPRT1 probe	Taqman	Hs99999909_m1
SSRP1 probe	Taqman	Hs01076277_g1
SUPT16H probe	Taqman	Hs01110649_g1
Biological samples		
Clinical samples of HCC patients	HKU, Queen Mary Hospital	N/A
Chemicals, peptides, and recombinant proteins		
Trizol	ThermoFisher	Cat#15596026
Lipofectamine 3000 transfection reagent	ThermoFisher	Cat#L3000001
Lipofectamine RNAiMAX reagent	ThermoFisher	Cat#13778150
EZ-link biotin-HPDP	ThermoFisher	Cat#21341
Dimethylformamide (DMF)	ThermoFisher	Cat#20673
No-Weight dithiothreitol (DTT) microtubes	ThermoFisher	Cat#20291
TCEP	ThermoFisher	Cat#T2556
Random hexamer primer	Invitrogen	Cat#N808012
1-β-d-ribofuranoside (DRB)	Sigma-Aldrich	Cat#D1916
4-thiouridine (4sU)	Sigma-Aldrich	Cat#T4509
Dimethyloxalylglycine (DMOG)	Sigma-Aldrich	Cat#D3695
Chlorhexidine (CHX)	Sigma-Aldrich	Cat#282227
VH298	Sigma-Aldrich	Cat#SML1896
MG132	Sigma-Aldrich	Cat#M7449
2-chloroacetamide (CAA)	Sigma-Aldrich	Cat#22790
Dynabeads MyOne streptavidin T1 beads	Life Technologies	Cat#65601
Curaxin CBL0137	Cayman	Cat#19110
HRP-conjugated secondary antibodies	Abcam	Cat#16912704, Cat#17028694

(*Continued on next page*)

Continued

REAGENT or RESOURCE	SOURCE	IDENTIFIER
Acetonitrile (ACN)	J.T. Baker	N/A
SYBR green qPCR master mix	Applied Biosystems	Cat#4309155
Taqman universal PCR master mix	Applied Biosystems	Cat#4304437
Complete protease inhibitor	Roche	Cat#04693116001
PhosSTOP phosphatase inhibitor cocktails	Roche	Cat#4906837001
Sorafenib	LC laboratories	Cat#S-8599
Cabozantinib	LC laboratories	Cat#C-8901
Lenvatinib	LC laboratories	Cat#L-5400
Bevacizumab	Selleckchem	Cat#A2006
Critical commercial assays		
Pierce ubiquitin enrichment kit	ThermoFisher	Cat#1859662
DNA-free DNA removal kit	ThermoFisher	Cat#AM1906
Hanging cell culture inserts	Millicell	Cat#MCHT24H48
pHrodo Red AM intracellular pH detection Kit	ThermoFisher	Cat#P35372
Dynabeads coIP kit	Invitrogen	Cat#14321D
2-NBDG glucose uptake assay kit	Biovision	Cat#K682-50
Lactate detection kit	Biovision	Cat#K607
Annexin V-FITC apoptosis detection kit	Vazyme	Cat#A211
miRNeasy kit	QIAGEN	Cat#217004
RNeasy MinElute cleanup kit	QIAGEN	Cat#74204
Anti-FLAG M2 agarose beads	Sigma-Aldrich	Cat#M8823
Deposited data		
RNA-seq data	This paper	PRJNA787102
Metabolites profiling by GC/MS	This paper	Table S5
Hydroxylation proline sites detected by LC-MS/MS	This paper	Table S4
RNA-Seq for tumors and corresponsding normal tissues	TCGA	www.cbioportal.org
Gene expression correlation in tumors	TCGA	http://gepia.cancer-pku.cn/index.html
Protein-protein interaction	HitPredict	http://www.hitpredict.org
Experimental models: Cell lines		
MHCC97L	Dr. ZY Yang	N/A
Huh7	Dr. Hidekazu Nakabayashi	N/A
HeLa	ATCC	Cat#CCL-2
MDA-MB-231	ATCC	Cat#HTB-26
ES2	ATCC	Cat#CRL-1978
HCT116	ATCC	Cat#CCL-247
HEK293	ATCC	Cat#CRL-11268
293FT	ATCC	Cat#CRL-1573
Experimental models: Organisms/strain		
C57BL/6 mice	Laboratory animal unit, the University of Hong Kong	N/A
BALB/c nude mice	Laboratory animal unit, the University of Hong Kong	N/A
Oligonucleotides		
Primers for quantitative PCR: listed in Table S1	This paper	
Primers for the construction of CRISPR plasmids: listed in Table S2	This paper	N/A
Primers for siRNA sequence: listed in Table S3	This paper	N/A

(*Continued on next page*)

Continued

REAGENT or RESOURCE	SOURCE	IDENTIFIER
Software and algorithms		
GraphPad Prism 5.0	GraphPad Prism Software	N/A
GraphPad Prism 7.0	GraphPad Prism Software	N/A
Pathway enrichment analysis	Enrichr online software	https://maayanlab.cloud/Enrichr/
TIDE	TIDE online software	https://tide.nki.nl
ImageJ 1.53k	NIH, USA	N/A
Image Lab 6.1	Image Lab Software	N/A
FlowJo V10	Flowjo Software	N/A

RESOURCE AVAILABILITY

Lead contact

Further information and requests for resources and reagents should be directed to and will be fulfilled by the Lead Contact Dr. Chun-Ming Wong (jackwong@pathology.hku.hk).

Materials availability

All unique/stable reagents generated in this study are available from the Lead Contact with a completed Materials Transfer Agreement.

Data and code availability

The genome-wide transcriptome sequencing under normoxia and hypoxia are available in SRA database: PRJNA787102. This paper does not generate original code. Any additional information required to reanalyze the data reported in this paper is available from the lead contact upon request.

EXPERIMENTAL MODEL AND SUBJECT DETAILS

Patient samples and cell lines

Totally 100 patients were involved in this study (Male to female ratio 4:1; average age: 57.3) Human HCC and their non-tumor liver tissues were surgically resected at Queen Mary Hospital and were snap-frozen in liquid nitrogen immediately after resection. Both tumor and non-tumor tissues were snap-frozen in liquid nitrogen and stored at −80°C. Prior acknowledgments were obtained from patients by signed consent for collection and usage of resected liver tissues. The use of human samples was approved by the institutional review board of the University of Hong Kong. Human HCC cell line MHCC97L was a gift from Dr. Z.Y. Tang (Fudan University). Huh-7 was obtained from Prof H. Nakabayshi (Hokkaido University). HeLa, MDA-MB-231, ES2, HCT116 and HEK293 were purchased from American Type Culture Collection. HeLa, HCT116, HEK293 and Huh-7 were cultured in Dulbecco's Modified Eagle Medium (DMEM) supplemented with 10% feta bovine serum (FBS, Gibco). MHCC97L, MDA-MB-231, and ES2 were cultured in DMEM with 10% FBS and 1% sodium pyruvate (NaPy, Gibco).

Establishment of the FACT complex and VHL knockout cells

For SSRP1 and SUPT16H knockout cells, we employed CRISPR gene editing system from Zhang Feng's lab. Cancer cells were first stably transfected Cas9. sgRNAs targeting SSRP1 or SUPT16H were transfected into MHCC97L, Huh-7, HeLa, MDA-MB-231, ES2, and HCT116, by lenti-viral approach. VHL knockout lines were established by the Alt-R CRISPR-Cas9 system with guide crRNAs designed to target VHL. Luciferase-labelled MHCC97L Cas9-WT, SSRP1 KO, SUPT16H KO were infected by transcend of tracrRNA and designed crRNA obtained from IDT. Knockout efficiencies were confirmed by Western blots and TIDE analysis. The sequences of the sgRNAs, crRNAs and siRNAs are listed in Tables S2 and S3.

Orthotopic liver implantation and hepatic artery ligation mice models

Hepatic artery ligation was performed by ligating the main branch of proper hepatic artery (PHA) under a dissection microscope. MHCC97L cells were orthotopically injected after ligation of the hepatic artery. 1×10^6 luciferase-labelled MHCC97L cells were injected into left lobes of the livers of 6-7-week-old male BALB/c nude mice. Mice were sacrificed between 4-5 weeks after surgery according to experimental design. Mice were administered with 100 mg/kg D-luciferin (Caliper) via intraperitoneal (i.p.) injection before bioluminescent imaging. Imaging was performed with Xenogen IVISTM100 Imaging System and quantified according to ROI values. Animal experiments were all carried out according to the Control of Hong Kong Animals Experiment Ordinance and the Institute's regulations on animal work.

In vivo drug treatment on mice models

Curaxin, Bevacizumab, Lenvatinib and Cabozantinib were used for *in vivo* drug treatments. 2 weeks after liver implantation of 1×10^6 luciferase labelled MHCC97L cells, mice were subjected to single or combined treatment of the following drugs according to experimental design. (1) vehicle with DMSO, (2) 30mg/kg or 15mg/kg Curaxin through oral gavage at 5-day-on/2-day-off schedule, (3) 5mg/kg Lenvatinib through oral gavage for 6 days per week, (4) 2mg/kg Cabozantinib through oral gavage 6 days per week, (5) 2mg/kg Bevacizumab by tail-vein injection twice per week. Body weights of mice were monitored for any significant adverse toxicity or side effects. After drug treatment for 2–3 weeks, mice were imaged with Xenogen system and sacrificed. Animal experiments were all carried out according to the Control of Hong Kong Animals Experiment Ordinance and the Institute's regulations on animal work.

Hydrodynamic tail vein (HDTV) injection mice models

p53 KO together with or without Supt16h KO by CRISPR-Cas9 and c-Myc OE by Sleeping Beauty transposon system plasmid were added to saline at a volume of 10% body weight. The plasmid mixture was then injected by tail vein of 6- to 8-week-old male C57BL/6N mice within 6-8 s. Mice were scarified after 4 weeks and livers were harvested. Tumor sizes were measured by a caliper and tumor volumes were calculated by length (mm) x width (mm) x depth (mm) × 0.5.

METHOD DETAILS

Knockdown of PHD1-3, HIF1A/HIF2A by siRNAs

For PHD1-3 knockdown model, MHCC97L cells were infected with PHD1-3 targeting siRNAs. For HIF1A and HIF2A knockdown model, FACT KO cells were infected with HIF1A or HIF2A targeting siRNAs. siNTC was used as control for all experiments. siRNAs were purchased from IDT and cells were infected at 5 μM siRNAs for 48 hours. Knockdown efficiencies were confirmed by RT-qPCR.

Transcriptome sequencing and pathway analysis

Transcriptome sequencing was performed in WT (2 replicas), SSRP1 KO sg#1, SSRP1 KO sg#4, SUPT16H KO sg#2, SUPT16H KO sg#3 MHCC97L cells that exposed to 20% and 1% O_2 for 24h. PolyA + mRNA library was prepared with TruSeq standard mRNA sample Prep kit (Illumina). 100 bp paired-end sequencing was performed by Illumina HiSeq2000. All data were analyzed by TopHat-Cufflinks pipeline and batch effects were corrected using RemoveBatchEffect from limma package. Gene pathway analysis were analyzed by online database Enrichr (https://maayanlab.cloud/Enrichr/) according to MSigDB-GSEA 2020 (Molecular Signatures Database).

Cell viability, proliferation, migration assay and colony formation assay

For cell viability assay, cells were seeded onto 6-well culture plate then cultured in 20% and 1% oxygen for 24–48 hours. Cells were stained with Crystal Violet and or counted by the Z1 coulter particle counter (Beckman Coulter). For proliferation assay, 2×10^4 cells were seeded onto 6-well cell culture plates in triplicate. Cell proliferation curve was measured by cell counting and cells were counted on a daily basis. Doubling time was calculated according to cell growth numbers upon co-silencing of HIF1A and the FACT complex. For cell migration assay, 2×10^5 cells were resuspended in FBS-free medium and seeded into the upper chamber of Transwell (Milicell, MCHT24H48). Growth medium was added in the bottom chamber. Cells were allowed to migrate for 24–48 hours. Bottom chambers were stained and pictured. For colony formation assay, 250–2000 cells were seeded onto 6-well culture plate. After incubation at 37°C for 2–3 weeks, the numbers of cell colonies were counted.

Reverse transcription quantitative PCR (RT-qPCR)

Total RNA extraction was performed with Trizol (ThermoFisher, 15596026) followed by reverse transcription with a random hexamer primer (Invitrogen, N808012). 18S was used as the internal normalization control for all experiments using SYBR Green qPCR Master Mix (Applied Biosystems) with specific primers in Table S1. RT-qPCRs of clinical samples were performed using Taqman Gene Expression Assay with SSRP1 and SUPT16H probes. HPRT1 probe was used as internal control. The level of target gene expression was determined using the ΔΔCt method for each comparison.

Protein extraction and Western blot

Cell lysates were collected with RIPA buffer containing protease inhibitor as standard protocol. Proteins were then resolved in SDS-PAGE and transferred onto nitrocellulose membrane. Antibodies listed in key resources table were used for detecting protein expression. β-actin was used as normalization control. Signals were detected with HRP-conjugated secondary antibodies (Abcam, 16912704, 17028694) and visualized with ECL detection reagent (GE Healthcare).

Intracellular pH detection

Intracellular pH level was determined with pHrodo Red AM (ThermoFisher, P35372). Cells were cultured under 20% and 1% O_2 for 2 days. After treatment, cells were washed with PBS and live cell imaging buffer, then labeled with pHrodo Red AM dye at 37°C for

30 minutes. After washing with live cell imaging buffer, cell fluorescence was measured by flow cytometry and confirmed by confocal imaging. Intracellular acidification level was quantified according to FITC intensity.

Glucose uptake assay

2-NBDG glucose uptake assay kit (Biovision, K682-50) was used to determine the glucose uptake ability of WT, SSRP1 KO, and SUPT16H KO cells under normoxic and hypoxic conditions. After incubation for 48 hours, cells were washed with PBS. 2-NBDG-FITC was added into each well and incubated at 37°C for 10 minutes. Level of 2-NBDG in cells were determined by flow cytometry and glucose uptake ability was calculated according to FITC intensity.

Lactate production

WT, SSRP1 KO, and SUPT16H KO MHCC97L cells were cultured under 20% and 1% O_2 for 24 hours. Culture medium was diluted according to the instruction from the manufacturer (Biovision, K607). Lactate enzyme mix was mixed with probe and assay buffer for each sample and incubated at room temperature for 30 minutes protected from light. Samples were measured using a microplate reader and lactate amount was calculated according to standard curve with normalization to cell number.

GC/MS metabolites profiling

For metabolic profiling and isotope labeling, culture medium with 25 mM [U-^{13}C] glucose or 25 mM ^{12}C glucose was replaced before incubation of cells under 20% and 1% O_2. After 24 hours, cells were washed with cold PBS and scraped into 0.8 mL ice-cold 80% methanol. Metabolites were extracted by three freeze-thaw cycles with liquid nitrogen. Samples were centrifuged at 14,000xg for 15 minutes to remove insoluble cell debris, and the supernatant was transferred to a new tube for centrifugal evaporation. A two-step derivatization method was used as previously described (Antoniewicz et al., 2007). Dried samples were dissolved in 30 μL of 20 mg/mL methoxyamine hydrochloride (Sigma) in pyridine (Sigma) and held at 37°C for 60 minutes. After dissolution and reaction, samples were incubated in 70 μL N,O-Bis-trimethylsilyl-trifluoroacetamide (BSTFA) plus 1% Trimethylchlorosilane TMCS (Sigma) at 55°C for 60 minutes. GC/MS analysis was performed using an Agilent 7890 GC equipped with a 30 m DB-35MS capillary column connected to an Agilent 5970B MS operating under electron impact ionization at 70 eV. 2 μL of sample was injected in splitless mode at 250°C using helium as the carrier gas at a flow rate of 1 mL/min. The GC oven temperature was held at 80°C for 1 minute and increased to 320°C at 10°/min, held at 320°C for 5 minutes. The transfer line temperature was set as 280°C. The MS detector recorded ion abundances in the range of 100–600 m/z (mass to charge ratio). Mass isotopomer distributions for glucose 6-phosphate (G6P), fructose 6-phosphate (F6P), phosphoenolpyruvic acid (PEP), pyruvate and lactate were determined by integrating ion fragments of 471–477 m/z, 147–150 m/z, 459–465 m/z, 217–220 m/z and 219–222 m/z, respectively. Data analysis was normalized to cell number accordingly and peak quantifications were performed using MassHunter Quantitative Analysis software (Agilent Technologies).

LC-MS/MS hydroxyproline site detection

HEK293 cells were overexpressed with FLAG-tagged SSRP1 and SUPT16H, followed by 8μM MG132 treatment together with or without DMOG treatment for 6 hours. Cells were then lysed in RIPA buffer. SSRP1 and SUPT16H protein werepurified by Anti-FLAG M2 agarose beads (Sigma, M8823). Protein samples were resolved using SDS-PAGE gel and targeted lanes were subjected to in-gel digestion. Protein digestion was performed by incubating with trypsin (1 ng/μL) at 37°C overnight. Subsequent tryptic peptides were pooled together and desalted using C18 StageTips for LC-MS/MS analysis. LC-MS/MS analysis was performed on Dionex Ultimate3000 nanoRSLC system coupled to Thermo Fisher Orbitrap Fusion Tribid Lumos Mass Spectrometer and raw mass spectrometry data were processed using MaxQuant 1.6.0.14. Raw data was searched against Uniprot human proteome database. Hydroxyproline, acetylation and oxidized methionine were selected as variable modification and cysteine carbamidomethylation was selected as a fixed modification. Confident proteins were identified using a target-decoy approach with a reversed database, strict false-discovery rate 1% at peptide and peptide spectrum matches level; minimum $\geq$2 unique peptides, $\geq$2 peptide spectral matches, localization probability score >0.75, Delta score >80.

Cell apoptosis assay

FACT KO or Curaxin-treated MHCC97L cells were cultured under 20% and 1% O_2 for 24 hours before harvest. Live cells and dead cells in culture medium were both collected and pelleted via centrifugation. Cells were washed by cold PBS and resuspended in binding buffer with annexin V–FITC and PI (Vazyme, A211) for staining according to the manufacturer's instructions. The percentage of cell apoptosis was analyzed with FACSCanto II Analyzer flow cytometry and FlowJo V10.

Transcription elongation assay

WT, SSRP1 KO, and SUPT16H KO cells were cultured under normoxic condition in a CO_2 incubator or hypoxic condition in a hypoxia workstation. After 4-hour incubation, 100 μM 5,6-dichlorobenzimidazole 1-β-d-ribofuranoside (DRB, Sigma-Aldrich, D1916) was added to the cells to temporally stop transcription. Cells were then incubated in DRB-contained culture medium under normoxic and hypoxic conditions for 3 hours. After washing out DRB, 1 mM 4-thiouridine (4sU, Sigma-Aldrich, T4509) was then used for labeling of the newly synthesized RNA. Total RNA of cell lines under indicated conditions was extracted after 0 min, 4 min, 8 min release

time. Total RNA was then extracted by Trizol as standard protocol. Biotinylation and purification of 4sU labeled RNA was done as described previously (Fuchs et al., 2015) using EZ-Link Biotin-HPDP (ThermoFisher Scientific, 21341) and captured using Dynabeads MyOne Streptavidin T1 beads (Life Technologies, 65,601). Magnetic beads were then fixed, cleaned and eluted with 100 μL of freshly prepared 100 mM dithiothreitol (DTT, ThermoFisher Scientific, 20291). RNA elusion was performed with RNeasy MinElute Kit (Qiagen) and eluted RNA samples were used for RT-qPCR with specific primers designed at 1-2 kb from TSS region and listed in Table S2.

Polyubiquitin pull-down assay

in vitro ubiquitination pull-down experiments were done with ubiquitin enrichment kit (Thermo Fisher, 89899) according to the manufacturer's instructions. Cells were first treated with MG132 at a final concentration of 8 μM for 8 hours to inhibit protein degradation. Protein samples were collected with RIPA buffer containing protease inhibitor and incubated in diluted ubiquitin affinity resin at 4°C overnight. Resin was collected by centrifugation and washed by washing buffer. Polyubiquitinated protein samples were eluted with SDS-PAGE loading buffer and detected with indicated antibodies listed in key resources table.

Immunoprecipitation of prolyl-hydroxylated proteins

Antibody coupling and immunoprecipitation was performed with Dynabeads coIP kit (Invitrogen, 14321D) according to the instructions from the manufacturers. N-terminal FLAG-tagged truncated forms of SSRP1 and SUPT16H in p3xFlag-CMV-10 backbones were transfected into HEK293 cells with lipofectamine 3000. Cells were treated with MG132 at a final concentration of 8μM for 8 hours before pull down. Hydroxyl-proline antibody was coupled to magnetic beads with a ratio of 5 μg antibody/mg beads. Protein lysates were incubated with antibody-conjugated beads at 4°C for 30 minutes. After washing, proteins were eluted by FLAG peptide and detected by Western blot.

Immunohistochemistry

Human and mouse livers and HCC tissues were fixed with 10% formalin and embedded in paraffin block. Paraffin sections were dewaxed with xylene and ethanol with standard protocols.

Antigen retrieval buffer (1 mM EDTA pH8.0) was boiled for 15 minutes. Sections were incubated with anti-KI67 (1:500, Abcam, ab1667) and anti-CD31 (1:200, Thermo Fisher, RB-10333) antibodies at dilution of 1:500 overnight at 4°C. After washing with TBST, the sections were incubated with horseradish peroxidase-conjugated secondary antibody (Dako) for 30 minutes at room temperature. IHC samples were developed with TBS diluted 3,3′-diaminobenzidine (Sigmal-Aldrich) and 30% w/w H_2O_2 and counterstained with haematoxylin.

Orthotopic liver implantation and hepatic artery ligation model

Hepatic artery ligation was performed by ligating the main branch of proper hepatic artery (PHA) under a dissection microscope. MHCC97L cells were orthotopically injected after ligation of the hepatic artery. 1×10^6 luciferase-labelled MHCC97L cells were injected into left lobes of the livers of 6-7-week-old male BALB/c nude mice. Mice were sacrificed between 4-5 weeks after surgery according to experimental design. Mice were administered with 100 mg/kg D-luciferin (Caliper) via intraperitoneal (i.p.) injection before bioluminescent imaging. Imaging was performed with Xenogen IVISTM100 Imaging System and quantified according to ROI values. Animal experiments were all carried out according to the Control of Hong Kong Animals Experiment Ordinance and the Institute's regulations on animal work.

In vivo drug treatment

Curaxin, Bevacizumab, Lenvatinib and Cabozantinib were used for *in vivo* drug treatments. 2 weeks after liver implantation of 1×10^6 luciferase labelled MHCC97L cells, mice were subjected to single or combined treatment of the following drugs according to experimental design. (1) vehicle with DMSO, (2) 30 mg/kg or 15 mg/kg Curaxin through oral gavage at 5-day-on/2-day-off schedule, (3) 5 mg/kg Lenvatinib through oral gavage for 6 days per week, (4) 2 mg/kg Cabozantinib through oral gavage 6 days per week, (5) 2 mg/kg Bevacizumab by tail-vein injection twice per week. Body weights of mice were monitored for any significant adverse toxicity or side effects. After drug treatment for 2–3 weeks, mice were imaged with Xenogen system and sacrificed. Animal experiments were all carried out according to the Control of Hong Kong Animals Experiment Ordinance and the Institute's regulations on animal work.

Hydrodynamic tail vein (HDTV) injection model

p53 KO together with or without Supt16h KO by CRISPR-Cas9 and c-Myc OE by Sleeping Beauty transposon system plasmid were added to saline at a volume of 10% body weight. The plasmid mixture was then injected by tail vein of 6- to 8-week-old male C57BL/6N mice within 6-8 s. Mice were scarified after 4 weeks and livers were harvested. Tumor sizes were measured by an caliper and tumor volumes were calculated by length (mm) × width (mm) x depth (mm) × 0.5.

Chemicals and drug dilution

Curaxin (CBL0137, 19110, Cayman) was dissolved in dimethyl sulfoxide (DMSO) for *in vitro* and *in vivo* use with indicated concentration. MG132 was added to cell culture medium at a final concentration of 8 μM for 4-8 h according to experimental design.

Cycloheximide (CHX) was used at a final concentration of 100 μg/mL for chase assay. Cells were treated with 1mM Dimethyloxalylglycine (DMOG) or 100 mM VH298 to stabilize HIFs. HCC drugs Sorafenib (LC Labs, S-8502), Cabozantinib (LC Labs, C-8901), and Lenvatinib (LC Labs, L-5400) were dissolved in DMSO for *in vitro* treatment. MHCC97L was treated with HCC drugs for 48 hours at 8 μM for Sorafenib, 10 μM for Lenvatinib, 10 nM for Cabozantinib. Bevacizumab (Selleckchem, A2006) was diluted with PBS and used at 300 μg/mL *in vitro* treatment on MHCC97L for 48 hours. Combined treatment was conducted with 100 nM Curaxin and DMSO was used as control.

QUANTIFICATION AND STATISTICAL ANALYSIS

Statistical analysis was performed using GraphPad Prism7 software. Data are expressed as mean ± standard deviation and analyzed by Student's t test. P values less than 0.05 were considered statistically significant.